2018

Impaired phloem loading in zmsweet13a,b,c sucrose transporter triple knock-out mutants in Zea mays

Margaret Bezrutczyk
Heinrich-Heine-Universitat Dusseldorf

Thomas Hartwig
Heinrich-Heine-Universitat Dusseldorf

Marc Horschman
Carnegie Institution of Science

Si Nian Char
Iowa State University

Jinliang Yang
University of Nebraska-Lincoln, jinliang.yang@unl.edu

See next page for additional authors

New Phytologist

Impaired phloem loading in *zmsweet13a,b,c* sucrose transporter triple knock-out mutants in *Zea mays*

Margaret Bezrutczyk[1,2,3], Thomas Hartwig[1,2,3], Marc Horschman[3], Si Nian Char[4], Jinliang Yang[5], Bing Yang[4], Wolf B. Frommer[1,2,3] and Davide Sosso[3]

[1]Institute for Molecular Physiology, Heinrich Heine University Düsseldorf, Düsseldorf 40225, Germany; [2]Max Planck Institute for Plant Breeding Research, Cologne 50829, Germany; [3]Department of Plant Biology, Carnegie Science, 260 Panama St, Stanford, CA 94305, USA; [4]Department of Genetics, Development, and Cell Biology, Iowa State University, Ames, IA 50011, USA; [5]Department of Agronomy and Horticulture, University of Nebraska-Lincoln, Lincoln, NE 68588, USA

Author for correspondence:
Wolf B. Frommer
Tel: +49 2118114826
Email: frommew@hhu.de

Received: *3 October 2017*
Accepted: *28 December 2017*

New Phytologist (2018) **218:** 594–603
doi: 10.1111/nph.15021

Key words: corn, efflux, export, leaf, maize (*Zea mays*), phloem loading, sucrose, transport.

Summary

- Crop yield depends on efficient allocation of sucrose from leaves to seeds. In Arabidopsis, phloem loading is mediated by a combination of SWEET sucrose effluxers and subsequent uptake by SUT1/SUC2 sucrose/H^+ symporters. ZmSUT1 is essential for carbon allocation in maize, but the relative contribution to apoplasmic phloem loading and retrieval of sucrose leaking from the translocation path is not known.
- Here we analysed the contribution of SWEETs to phloem loading in maize.
- We identified three leaf-expressed SWEET sucrose transporters as key components of apoplasmic phloem loading in *Zea mays* L. ZmSWEET13 paralogues (a, b, c) are among the most highly expressed genes in the leaf vasculature. Genome-edited triple knock-out mutants were severely stunted. Photosynthesis of mutants was impaired and leaves accumulated high levels of soluble sugars and starch. RNA-seq revealed profound transcriptional deregulation of genes associated with photosynthesis and carbohydrate metabolism. Genome-wide association study (GWAS) analyses may indicate that variability in ZmSWEET13s correlates with agronomical traits, especifically flowering time and leaf angle.
- This work provides support for cooperation of three ZmSWEET13s with ZmSUT1 in phloem loading in *Z. mays*.

Introduction

Crop yield is critical for human nutrition, yet the underlying machinery that ultimately determines yield potential is still not understood. Crop productivity under ideal conditions is determined by the efficiency with which plants intercept light, convert it into chemical energy, translocate photosynthates and convert these to storage products in harvestable organs (Zhu *et al.*, 2010). In many crops, sucrose is the primary form for translocation inside the conduit (i.e. the phloem). A combination of SWEET-mediated efflux from phloem parenchyma and subsequent secondary active sucrose import by SUT sucrose/H^+ symporters is thought to create the driving force for pressure gradient-driven phloem transport and retrieval of sucrose leaking along the translocation path (Chen *et al.*, 2015a).

Sucrose is thought to follow one of three routes during phloem loading: (1) apoplasmic loading via plasma membrane transporters, (2) symplasmic loading via diffusion through plasmodesmata or (3) polymer trapping via enzymatic addition of galactose, which is thought to impair back-diffusion through plasmodesmata (Turgeon & Wolf, 2009; Chen *et al.*, 2015a). Some mechanisms may coexist, as suggested by anatomical studies which have found thin- and thick-walled sieve tubes in monocots, cell types that may differ regarding the primary loading mechanism (Botha, 2013).

In Arabidopsis, a SWEET/SUT-mediated apoplasmic mechanism appears to be important for phloem loading (Chen *et al.*, 2012, 2015a). SWEETs are a class of transporters with seven transmembrane helices that function as hexose or sucrose uniporters (Xuan *et al.*, 2013). Multiple SemiSWEETs and SWEETs have been crystallized, and AtSWEET13 has been proposed to function in complexes via a 'revolving door' mechanism to accelerate transport efficacy (Feng & Frommer, 2015; Han *et al.*, 2017; Latorraca *et al.*, 2017). In Arabidopsis, SWEET roles include phloem loading, nectar secretion, pollen nutrition and seed filling (Chen *et al.*, 2012; Sun *et al.*, 2013; Lin *et al.*, 2014; Sosso *et al.*, 2015). In rice, cassava and cotton, SWEETs act as susceptibility factors for pathogen infections (Chen *et al.*, 2010; Cohn *et al.*, 2014; Cox *et al.*, 2017). AtSWEET11 and 12 are probably responsible for effluxing sucrose from the phloem parenchyma into the apoplasm (Chen *et al.*, 2012). Sucrose is subsequently loaded against a concentration gradient into the sieve element companion cell complex (SECC) via the SUT1 sucrose/H^+ symporter (a.k.a. AtSUC2), powered by the proton gradient created by co-localized H^+/ATPases (Riesmeier *et al.*, 1994; Gottwald *et al.*, 2000; Slewinski *et al.*, 2009; Srivastava *et al.*, 2009). Although the fundamental

involvement of SUT transporters in phloem loading has been demonstrated using RNA interference (RNAi) and knock-out mutants in Arabidopsis (also in potato, tobacco, tomato and maize) (Riesmeier *et al.*, 1994; Bürkle *et al.*, 1998; Srivastava *et al.*, 2009; Chen *et al.*, 2015a), *atsweet11,12* and *atsuc2 (sut1)* mutants were able to produce viable seeds and only showed a slight reduction in plant growth (Chen *et al.*, 2012).

In monocots, including all cereal crops, the situation is less clear. In maize, the phloem-expressed ZmSUT1 (Baker *et al.*, 2016) (phylogenetically in the SUT2 clade) appears to be critically important for phloem translocation (Slewinski *et al.*, 2009), whereas rice *ossut1* mutants and RNAi lines had no apparent growth or yield defects (Ishimaru *et al.*, 2001; Scofield *et al.*, 2002; Eom *et al.*, 2012). As a result, there is an ongoing debate regarding the mechanisms behind phloem loading in cereals (Braun *et al.*, 2014; Regmi *et al.*, 2016).

Here we identified a set of three close paralogs of SWEET13 from *Zea mays* L. as essential transporters for efflux of sucrose into the apoplasm before phloem loading.

Materials and Methods

Plant material and growth conditions

zmsweet13a, *zmsweet13b* and *zmsweet13c* alleles were obtained with a CRISPR-Cas9 construct targeting a sequence (5′-GCATCTACAAGAGCAAGTCGACGG-3′, the underlined CGG for PAM) conserved in all three paralogs in the 3rd exon using a CRISPR system and associated method as described (Char *et al.*, 2017). Briefly, a pair of 24-nt oligonucleotides matching to the target site were synthesized and annealed into a double-stranded DNA fragment. The DNA fragment was subcloned into an intermediate vector pgRNA1 and the resulting guide RNA expression cassette was mobilized into the Cas9 expressing binary vector pGW-Cas9 through the Gateway recombination reaction using the recombinase, resulting in pCas9-gRNA_SWEET13. The CRISPR construct was transformed into the *Agrobacterium tumefaciens* strain EHA101 for plant transformation. Maize transformation was performed at the Iowa State University Plant Transformation Facility. Hi-II calli were derived from the F_1 immature embryos of Hi-IIA and Hi-IIB plants, which are independent lines of a B73xA188 cross. Calli were transformed with *A. tumefaciens* containing plasmids for expressing guide RNAs and the Cas9 construct. T0 plantlets grown on sterile media from successfully transformed calli were transplanted to soil when 1 inch in height. T0 plants were selfed or outcrossed to B73, and plants which did not contain the CRISPR construct were selected by performing PCR using three different primer pairs targeting Cas9 (Supporting Information Table S1). T1, T2 and T3 plants homozygous for all three mutated genes (*zmsweet13abc*) were selected along with wild-type siblings. Height was assessed by weekly measurement from the soil surface to the top of the highest fully developed leaf. Wild-type 'siblings' were descendants of the Hi-II plants transformed and outcrossed once to B73, which in the T1 generation did not carry the CRISPR-Cas9 construct or any detectable mutations. Triple mutant plants either descended from selfed T0 Hi-II plants or outcrossed once to B73. The mutant phenotype was unaffected by the difference in genetic background. Mutants and wild-type plants were grown side by side, in glasshouses under long-day conditions (16 h : 8 h, day : night, 28–30°C), and in 2016 in a summer field at Carnegie Science (Stanford, CA, USA).

Genotyping of maize plants

Genomic DNA was extracted from leaves using a Qiagen Biosprint 96 device. PCR was performed with the Terra PCR Direct Red Dye Premix Protocol (Clontech Laboratories, Palo Alto, CA, USA) with melting temperatures of 60, 64 and 62.5°C for *ZmSWEET13a*, *b* and *c*, respectively (for primers see Table S1). Amplicons of relevant regions of the CRISPR-Cas9 targeted *ZmSWEET13* alleles were sequenced by Sequetech (Mountain View, CA, USA). Chromatograms were analysed using 4Peaks (www.nucleobytes.com/4peaks/).

Plastic embedding and sectioning

Flag leaves collected at 07:00 h were placed in 0.1 M cacodylate-buffered fixative with 2% paraformaldehyde and 2% glutaraldehyde, vacuum infiltrated for 15 min and incubated overnight. Sample dehydration was performed by a graded ethanol series (10, 30, 50, 70 and 95%). Sample embedding was performed according to the LR White embedding kit protocol (Electron Microscopy Science, Hatfield, PA, USA). Cross-sections (1.5 μm) were obtained on an Ultracut (Reichert, Depew, NY, USA), stained for 30 s with 0.1% toluidine blue and washed with double distilled H_2O (2×), followed by 5 min of starch staining with saturated Lugol's solution. Sections were mounted with CytoSeal 60 (Electron Microscopy Science).

Phylogenetic analyses

The evolutionary history was inferred by using maximum likelihood with a JTT matrix-based model. The tree with the highest log likelihood (−3000.1) is shown. The percentage of trees in which associated taxa clustered together is shown next to the branches. Initial tree(s) for the heuristic search were obtained by neighbour-joining to a matrix of pairwise distances with the JTT model used for estimation. The analysis involved 16 polypeptide sequences, derived from Phytozome (https://phytozome.jgi.doe.gov) and Gramene (http://www.gramene.org/) using *ZmSWEET13a* as a template in a search for similar sequences in the genomes of *Z. mays*, *Sorghum bicolor*, *Setaria italica*, *Hordeum vulgare*, *Triticum urartu* (progenitor of A-genome of bread wheat *Triticum aestivum*), *Brachypodium distachyon* and *Oryza sativa*. A minimum of 95% site coverage was required so that no more than 5% alignment gaps, missing data and ambiguous bases were allowed at any position. There were a total of 252 positions in the final dataset. Evolutionary analyses were conducted in Mega6.

Soluble sugar analyses

Flag leaves were harvested from mature plants at 07:00 h. In total, 70 mg of liquid nitrogen-ground tissue was incubated for

1 h with 1 ml of 80% ethanol on ice with frequent mixing. Samples were centrifuged for 5 min at 4°C at 13 000 ***g***, and supernatant was removed. This step was repeated once. The liquid supernatant was subsequently dried in a vacuum concentrator and re-suspended in water. Sucrose, glucose and fructose were measured using NADPH-coupled enzymatic methods using an M1000 plate reader (Tecan, Männedorf, Switzerland), with measured values normalized to fresh weight. Starch quantification was performed as previously described (Sosso *et al.*, 2015).

Starch staining

Flag leaves collected at 07:00 h were boiled in 95% ethanol for *c.* 30 min (until chlorophyll pigments disappeared). Cleared leaves were submerged in saturated Lugol's iodine solution for 15 min, rinsed twice with H_2O and imaged with a Lumix GF1 camera (Panasonci, Kadoma, Osaka, Japan). The IKI solution used for starch staining was made by adding 1 g of iodine and 1 g of potassium iodide to 100 ml H_2O.

qRT-PCR RNA isolation and transcript analyses

RNA was extracted using the Trizol method (Invitrogen). First-strand cDNA was synthesized using a Quantitect reverse transcription kit (Qiagen). Quantitative reverse transcriptase PCR (qRT-PCR) to determine expression level was performed using a LightCycler 480 (Roche), and the $2^{-\Delta Ct}$ method for relative quantification. Wild-type maize and *zmsweet13abc* flag leaves were sampled at 17:00 h. Primers in the last exon and the 3′ untranslated region of *ZmSWEET13a, b* and *c* (Table S1) were used for qRT-PCR to determine gene expression levels. Internal references were *Zm18s* and *ZmLUG*.

FRET sucrose sensor analysis in HEK293T cells

ZmSWEET13a, b and *c* coding sequences were cloned into the Gateway entry vector pDONR221f1, followed by LR (*att*L, *att*R) recombination into pcDNA3.2V5 for expression in HEK293T cells. HEK293T cells were co-transfected with *ZmSWEET13a, b* or *c* in *pcDNA3.2V5* and the sucrose sensor FLIPsuc90μΔ1V (Chen *et al.*, 2012) using Lipofectamine 2000 (Invitrogen). For fluorescence resonance energy transfer (FRET) imaging, Hank's balanced salt solution medium was used to perfuse HEK293T/FLIPsuc90μΔ1V cells with defined pulses containing 20 mM sucrose in buffer. Image acquisition and analysis were performed as previously described (Chen *et al.*, 2012). AtSWEET12 was used as a positive control. Negative controls were empty vector transfectants.

Transient gene expression in *Nicotiana benthamiana* leaves

The *A. tumefaciens* strain GV3101 was transformed with the binary expression clone (pAB117) carrying *ZmSWEET13a*, *b* or *c* C-terminally fused with enhanced green fluorescent protein (eGFP) and driven by the CaMV 35S promoter. *Agrobacterium* culture and tobacco leaf infiltration were performed as described (Sosso *et al.*, 2015). Chloroplast autofluorescence was detected on a Leica TCS SP8 confocal microscope with 488 nm excitation (eGFP) and 561 nm excitation (chlorophyll). Emission was detected at 522–572 nm (eGFP fluorescence) and 667–773 nm (chloroplast fluorescence). Epidermal leaf chloroplast fluorescence (Dupree *et al.*, 1991) allowed us to determine eGFP vacuolar localization (lining chloroplasts on the vacuolar side) and plasma membrane localization was deduced (peripheral to chloroplasts; according to bright-field image). Image analysis was performed using Fiji software (https://fiji.sc/).

Analyses of photosynthetic rates

Licor LI-6800 measurements were taken at mid-day under glasshouse conditions (28°C, photosynthetically active radiation (PAR) 1000 μE m^{-2} s^{-1}, 60% relative humidity). Two-centimetre-diameter discs of leaves were clamped in the Licor measurement chamber and relative concentrations of CO_2 inside and outside of the chamber were measured. CO_2 absorbed (μmol m^{-2} s^{-1}) by leaf segments in the chamber was used as a proxy for photosynthetic rate. Measurements were made at the tips of leaf 7 to leaf 10 at midday.

Candidate gene association study

To test whether sequences at *SWEET* loci are associated with phenotypic variations in the maize population, we analyzed a maize diversity panel composed of 282 inbred lines (HapMap3 SNP data (Bukowski *et al.*, 2017) for the panel from the Panzea database (www.panzea.org)). We filtered single nucleotide polymorphism (SNP) data (minor allele frequency (MAF) > 0.1; missing rate < 0.5) using Plink (Purcell *et al.*, 2007) and calculated a kinship matrix with Gemma (Zhou & Stephens, 2012) using the filtered SNP set. A genome-wide association study (GWAS) was performed by fitting a mixed linear model using Gemma, where the kinship matrix was fitted as random effects in the model. A false discovery rate (FDR) approach (Benjamini & Hochberg, 1995) was used to control the multiple test problem with a cut off of 0.05. Linkage disequilibrium of SNPs in our candidate genes with significant association SNPs was calculated using Plink (Purcell *et al.*, 2007).

RNA-seq and data analysis

zmsweet13abc triple mutants and wild-type siblings were grown in soil under glasshouse conditions. Total RNA was isolated from flag leaf tissues using acidic phenol extraction as described previously (Eggermont *et al.*, 1996). Purification of poly-adenylated mRNA using oligo(dT) beads, construction of barcoded libraries and sequencing using Illumina HiSeq technology (150 bp paired-end reads) were performed by Novogene (https://en.novogene.com/) using the manufacturer's recommendations. Trimmed and quality control-filtered sequence reads were mapped to the B73 AGPv3 genome using Star (v.2.54) (Dobin *et al.*, 2013) in two pass mode (parameters: –outFilterScoreMinOverLread 0.3, –outFilterMatchNminOverLread 0.3, –outSAMstrandField intronMotif, –outFilterType BySJout, –outFilterIntronMotifs RemoveNoncanonical, –quantMode TranscriptomeSAM GeneCounts). To obtain

uniquely mapping reads, these were filtered by mapping quality (q20), and PCR duplicates were removed using SAMTOOLS (v.1.3.1). Gene expression was analysed in R (v.3.4.1) using DESEQ2 software (v.1.16.1) (Love *et al.*, 2014). Genes were defined as differentially expressed by a two-fold expression difference with a *P*-value, adjusted for multiple testing, of < 0.05 (Fig. S7; Table S2). RNA-seq data are available in the NCBI Gene Expression Omnibus database.

Results

To test whether SWEETs are involved in phloem loading in maize, we evaluated the role of leaf-expressed maize *SWEETs* in carbon allocation. We identified three *SWEET13* paralogs (GRMZM2G173669: *ZmSWEET13a*, GRMZM2G021706: *ZmSWEET13b*, GRMZM2G179349: *ZmSWEET13c*) as the most highly expressed SWEETs in maize leaves based on published expression values in four publicly available datasets (Denton *et al.*, 2017) (Fig. S1). *ZmSWEET13a* and *b* are located in tandem on chromosome 10 in a region syntenic with the *OsSWEET13* locus in rice, while *ZmSWEET13c* is on chromosome 3 (Fig. S2). Interestingly, maize is one of the few cereals having three *SWEET13* paralogs, along with *Sorghum bicolor* and *Triticum urartu* (Figs 1a, S3). Similar to ZmSUT1, *ZmSWEET13a, b* and *c* mRNA preferentially accumulated in bundle sheath/vein preparations rather than mesophyll (Fig. 2a). If the SWEETs were involved in phloem loading, one would expect that their mRNA levels would be highest in leaf domains that serve as sucrose sources, as compared to sink tissues. Consistent with a role in phloem loading, mRNA levels of all three *SWEET13*s (as well as *SUT1*) were highest in leaf tips (Fig. 2b). Analysis of independent RNA-seq experiments that had differentiated source and sink regions of maize leaves on the basis of radiotracer experiments also found *ZmSWEET13* transcripts to be ~ five-fold higher in source vs sink domains (Fig. S4) (Wang *et al.*, 2014). We tested the transport activity of the three SWEETs in human HEK293T cells coexpressing a genetically encoded sensor (Chen *et al.*, 2010, 2012). All three SWEETs mediated sucrose transport (Fig. 1b). To test whether these SWEETs were part of (1) intercellular translocation or (2) intracellular sugar sequestration similar to Arabidopsis SWEET2, 16 or 17 (Chardon *et al.*, 2013; Klemens *et al.*, 2013; Guo *et al.*, 2014; Chen *et al.*, 2015b), we tested their subcellular localization in transiently transformed tobacco cells, and found that they localized preferentially to the plasma membrane (Fig. 1c).

Recently, *ZmSWEET13* had been implicated as a possible key player in C_4-photosynthesis in grasses (Emms *et al.*, 2016). To test their role in maize, we designed guide RNAs that target a conserved region within a transmembrane domain, assuming that defects in the membrane domain would lead to complete loss of function. We generated single *knock-out* mutants, as well as

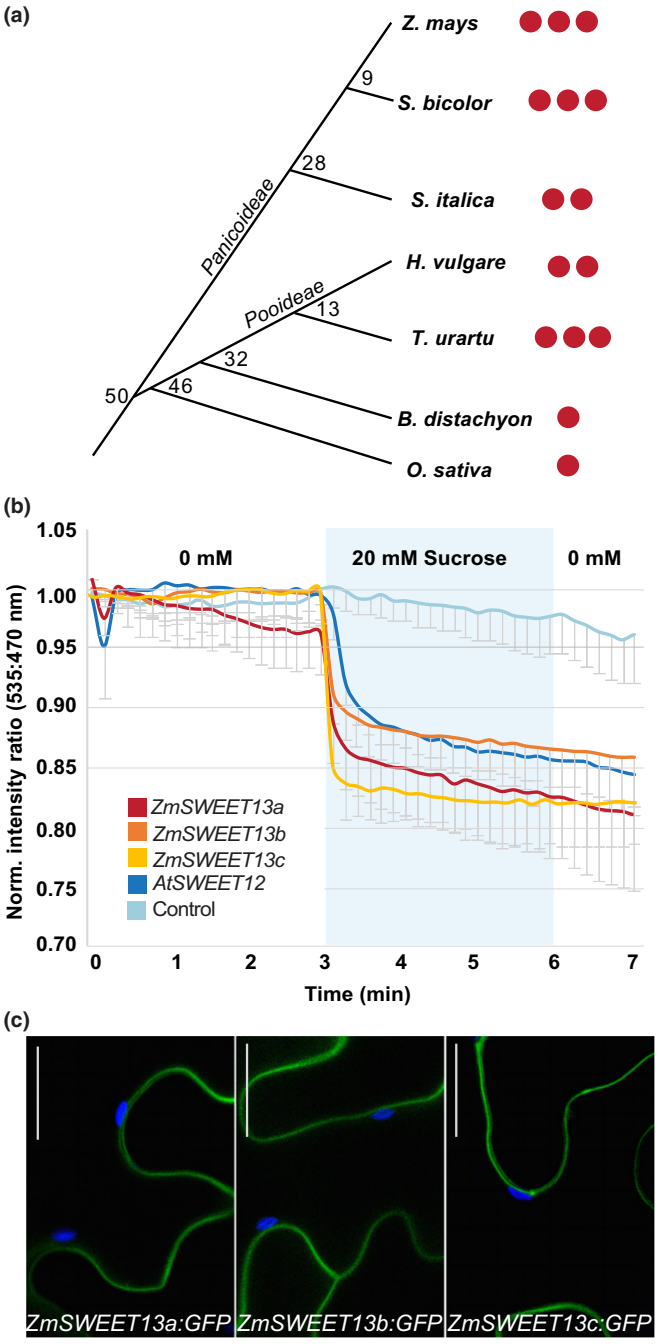

Fig. 1 Phylogeny, functional analysis and subcellular localization of SWEET13a,b,c. (a) Phylogenetic relationship between putative orthologs in the following grasses: *Zea mays* L., *Sorghum bicolor*, *Setaria italica*, *Hordeum vulgare, Triticum urartu* (progenitor of A-genome of bread wheat *Triticum aestivum*), *Brachypodium distachyon* and *Oryza sativa*. Chronogram branch divergence time-points are in million years (Emms *et al.*, 2016). Red dots represent the number of *SWEET13* paralogs for each species. (b) Sucrose transport activity by ZmSWEET13a, b and c in HEK293T cells coexpressing FLIPsuc90μΔ1V (fluorescent sucrose sensor). Cells were transfected to express sensors only as negative control, or to co-express *AtSWEET12* as a positive control. HEK293T cells were perfused with buffer, then subjected to a 3-min pulse of 20 mM sucrose (mean ± SEM, repeated independently four times with comparable results). (c) Confocal images (maximum projection of Z-stack) of *Agrobacterium*-infiltrated *Nicotiana benthamiana* epidermal leaf cells transiently expressing ZmSWEET13a-eGFP, ZmSWEET13b-eGFP or ZmSWEET13c-eGFP fusions. The eGFP emission (green, 522–572 nm) was merged with chloroplast fluorescence (blue, 667–773 nm). ZmSWEET13x-eGFP derived fluorescence between chloroplasts and the cell periphery indicates localization to the plasma membrane. Bars, 50 μm.

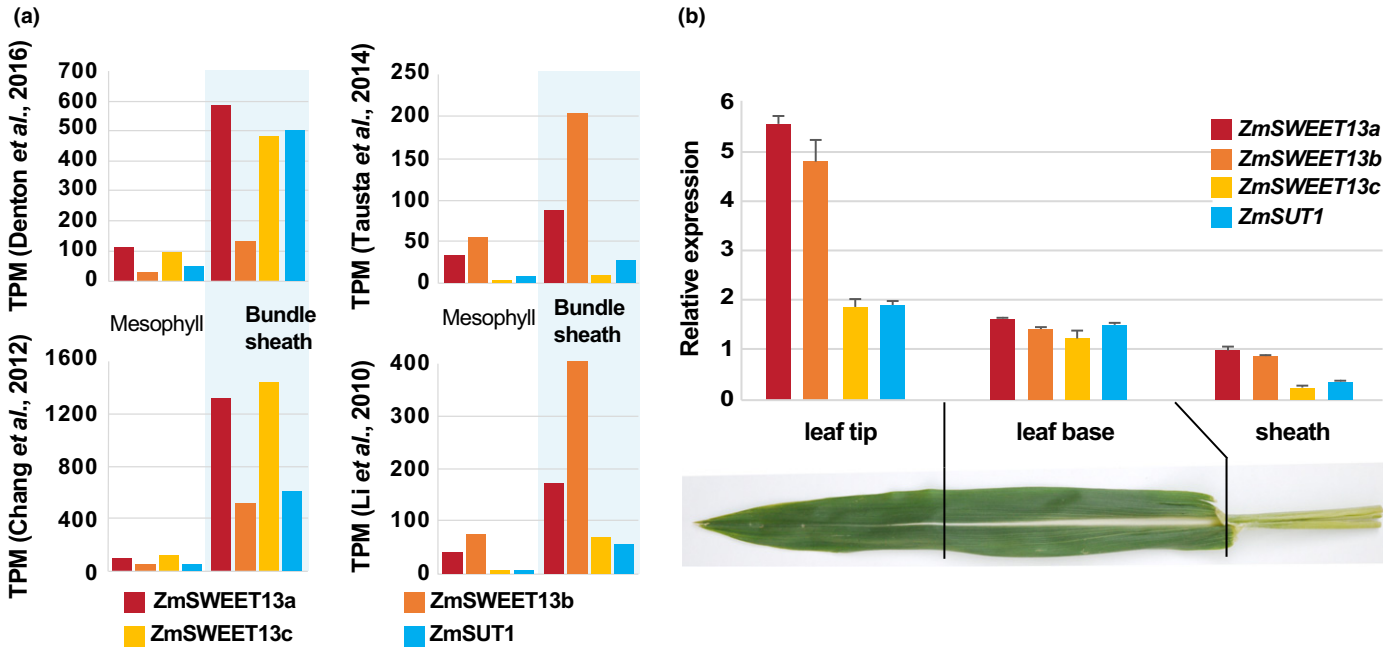

Fig. 2 *ZmSWEET13*s and *ZmSUT1* mRNA levels in flag leaves of *Zea mays* L. (a) *ZmSWEET13*a,b,c and *ZmSUT1* mRNAs accumulate preferentially in the bundle sheath and vein preparations, relative to mesophyll in four independent datasets (Li *et al.*, 2010; Chang *et al.*, 2012; Tausta *et al.*, 2014; Denton *et al.*, 2017) (TPM, transcripts per million; see also Supporting Information Fig. S1). (b) Relative mRNA levels (by qRT-PCR) of *ZmSWEET13a, b, c* and *ZmSUT1* in maize flag leaves. All four genes had highest mRNA levels in leaf tips (mean ± SEM, $n = 3$ technical replicates with expression normalized to *Zm18S* transcript levels, repeated independently four times with comparable results, see Fig. S13e, f).

combinations of mutant alleles, using CRISPR-Cas9 (Fig. 3). We recovered two mutant alleles of *ZmSWEET13a*, four of *ZmSWEET13b* and three of *ZmSWEET13c*. The majority of mutations were caused by single nucleotide insertions in the target sequence. All mutations created premature stop codons leading to truncated polypeptides at amino acid 129 in the fourth of seven transmembrane domains (Fig. 3). T2 lines carrying homozygous mutations in all three genes were characterized by severe growth defects (Fig. 4a). The growth phenotype was analyzed in subsequent generations in the glasshouse and in a single field season. Single and double mutants showed slight growth defects, while triple mutants had substantial defects: plants were severely stunted with shorter, narrower leaves (Fig. 4a–c). Leaves were chlorotic, and accumulated ~5× more starch and ~4× more soluble sugars compared to the wild-type (Fig. 5a–c), consistent with symptoms expected for impaired phloem loading. Accumulation of starch occurred primarily in mesophyll and bundle sheath cells (Fig. 5d, e). As observed in plants with impaired phloem loading, photosynthesis was also strongly impacted in glasshouse-grown *zmsweet13a,b,c* mutants (Fig. S5). In the field, triple mutants from five independent allelic combinations presented even more severe phenotypes, with extreme chlorosis, massive anthocyanin accumulation and extremely stunted growth; in several cases this resulted in lethality (Fig. 4e). *SWEET13* mRNA levels were drastically reduced in all three *ZmSWEET13s*, as quantified by RNA-seq and qRT-PCR (Figs 4d, S6). In summary, the strong phenotype of the triple mutants is consistent with maize using predominantly an apoplasmic phloem loading mechanism.

Despite the severe defects, triple mutant plants grown in the glasshouse (as well as a subset in the field) exported sufficient sugars from leaves to produce viable seeds. A possible explanation for the viability of the triple mutants could be compensation by other sucrose-transporting clade III SWEETs. To test this hypothesis and to obtain insights about possible physiological changes in the mutants, we performed an RNA-seq analysis of flag leaves of wild-type (Hi-II transformants outcrossed once to B73 and selfed that neither contain SWEET13 mutations nor contain Cas9 as verified by PCR) and triple mutant plants (Hi-II background) (Fig. S7). Notably, we did not observe significant enrichment of mRNA of any of the clade III *SWEETs*, arguing against transcriptional compensation by other clade III *SWEETs* (Fig. S6). Our data do not exclude the possibility that compensation occurs at the post-transcriptional level. We performed a pathway enrichment analysis using the Plant MetGenMap database (Joung *et al.*, 2009) and found that mRNA levels of multiple genes encoding functions in the light-harvesting complex and in chlorophyll/tetrapyrrole biosynthesis were substantially reduced in triple mutants, consistent with impaired photosynthesis and chlorosis (Figs S8, S9). Furthermore, in line with the accumulation of starch and soluble sugars in leaves, transcripts related to carbohydrate synthesis and degradation, in particular starch biosynthesis and sucrose degradation, were affected in the triple mutants (Fig. S10; Table S3).

A recent study has found that the Arabidopsis homolog AtSWEET13 (although phylogenetically not the closest homolog of ZmSWEET13) can also transport gibberellin (Kanno *et al.*, 2016). The observed phenotypes of the triple *zmsweet13 knock out* mutants in maize are consistent with a primary role in sucrose transport and distinct from those observed in the Arabidopsis

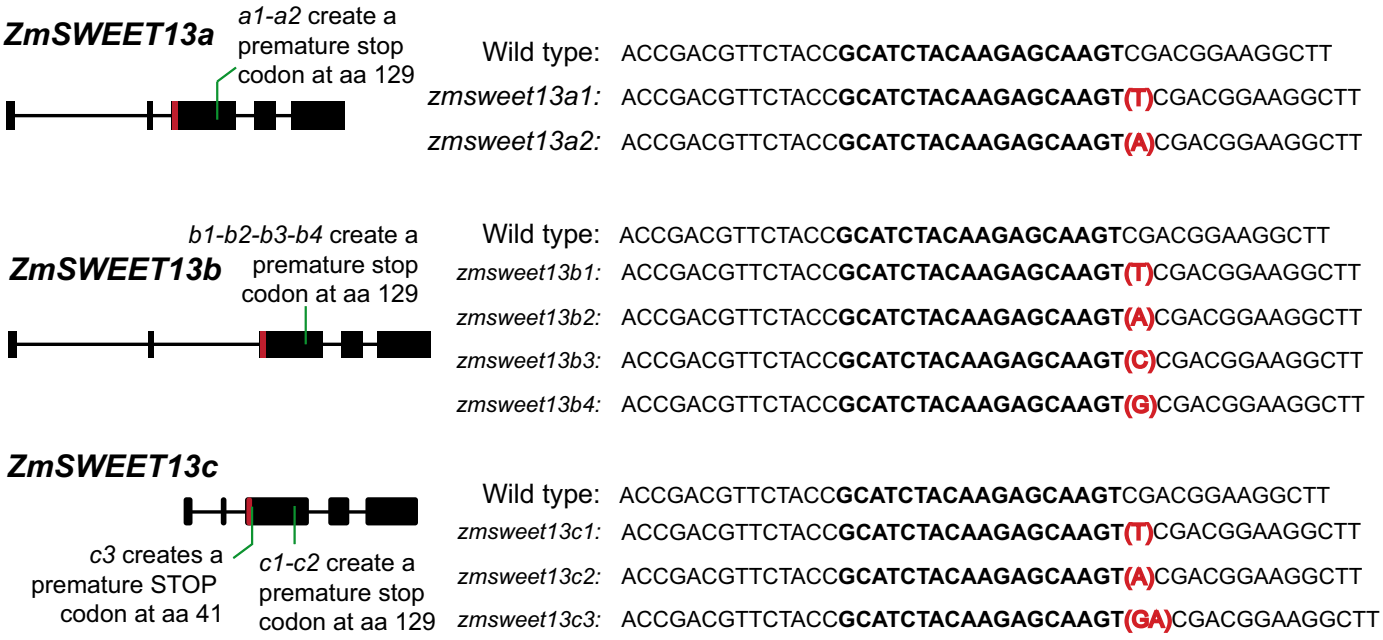

Fig. 3 CRISPR-Cas9-induced *ZmSWEET13a, b* and *c* mutations in *Zea mays* L. Schematic representation of *ZmSWEET13a*, *b* and *c* gene models, with exons displayed as black boxes. Schematics of the target site within the third exon (red) and sequences of the insertions obtained by genomic editing by CRISPR-Cas9, as determined in T3 homozygous lines, with guide RNAs marked in bold. The nine alleles carry frameshift mutations with insertions of either 1 or 2 nt, resulting in premature stop codons, as indicated within the gene model by a green line.

sweet13;14 double mutant, namely male sterility, and increased seedling and seed size (Kanno *et al.*, 2016).

To determine if variation in the *ZmSWEET13* genes may account for differences in agronomically important traits in existing maize lines, we conducted a GWAS using phenotypic traits obtained from a maize diversity panel (Flint-Garcia *et al.*, 2005). We obtained genotypic data from maize HapMap3 SNPs (Bukowski *et al.*, 2017) and filtered out SNPs with a minor allele frequency < 0.1 and missing rate > 0.5, leaving ~13 million SNPs for analyses. We performed GWAS using a mixed linear model approach (Zhou & Stephens, 2012), where kinship calculated from the genome-wide SNPs was fitted as the random effects. The SNPs that passed the FDR threshold of 0.05 and showed linkage disequilibrium ($R^2 > 0.8$) with *ZmSWEET13a,b,c* genes were considered significant associations. SNPs in *ZmSWEET13s* were significantly associated with ear-related traits (i.e. ear rank number and ear height) and developmental traits (i.e. days to silk, days to tassel, middle leaf angle and germination count) (Figs S11, S12). While these results are compatible with a key role of *ZmSWEET13s* in carbon allocation, it will be necessary to determine whether polymorphisms in these genes or flanking regions are causative for these traits.

Discussion

The phloem sap of many monocots and dicots contains high sucrose concentrations. The high sucrose contents in the loading zone are thought to create a pressure gradient that drives phloem translocation. Inhibition of the expression of the SUT1 sucrose/H^+ symporter by RNAi or T-DNA insertion typically leads to stunted growth and accumulation of carbohydrates in leaves (Riesmeier *et al.*, 1994; Bürkle *et al.*, 1998; Gottwald *et al.*, 2000; Slewinski *et al.*, 2009; Srivastava *et al.*, 2009). Chlorosis and inhibition of photosynthesis, which often accompany defects in phloem translocation, may either be due to feedback inhibition of photosynthesis or be a consequence of nutrient deficiencies caused by the reduced supply of carbohydrates to the root system (Ainsworth & Bush, 2011). SUTs function as sucrose/H^+ symporters and, at least in maize, appear to fulfil two roles: (1) loading of the SECC with sucrose in source leaves, and (2) retrieval of sucrose that diffuses out of the SECC, as a consequence of the high sucrose concentration in the SECC, relative to surrounding tissues. SUTs import sucrose from the cell wall space, implying the existence of transporters that efflux sucrose into the cell wall space preceding uptake by SUTs. AtSWEET11 and 12 are candidates for such an efflux role in Arabidopsis: they appear to function as uniporters and can thus serve as cellular efflux systems when sucrose gradients are suitable. Both SWEETs were highly expressed in leaves, localized most likely to the phloem parenchyma, and *atsweet11;12* mutants were smaller and accumulated starch in leaves (Chen *et al.*, 2012). However, the phenotype of *atsweet11;12* mutants was relatively weak, implying leaky mutations, compensation by other transporters or the coexistence of other phloem loading mechanisms. Other mechanisms could include symplasmic transport, or yet unknown processes.

Here, we show that maize has three closely related clade III SWEETs (named SWEET13a, b and c) that are encoded by some of the most highly expressed genes in the leaf. The three genes possibly derive from relatively recent gene duplication events: sorghum and wheat have three copies per genome, while

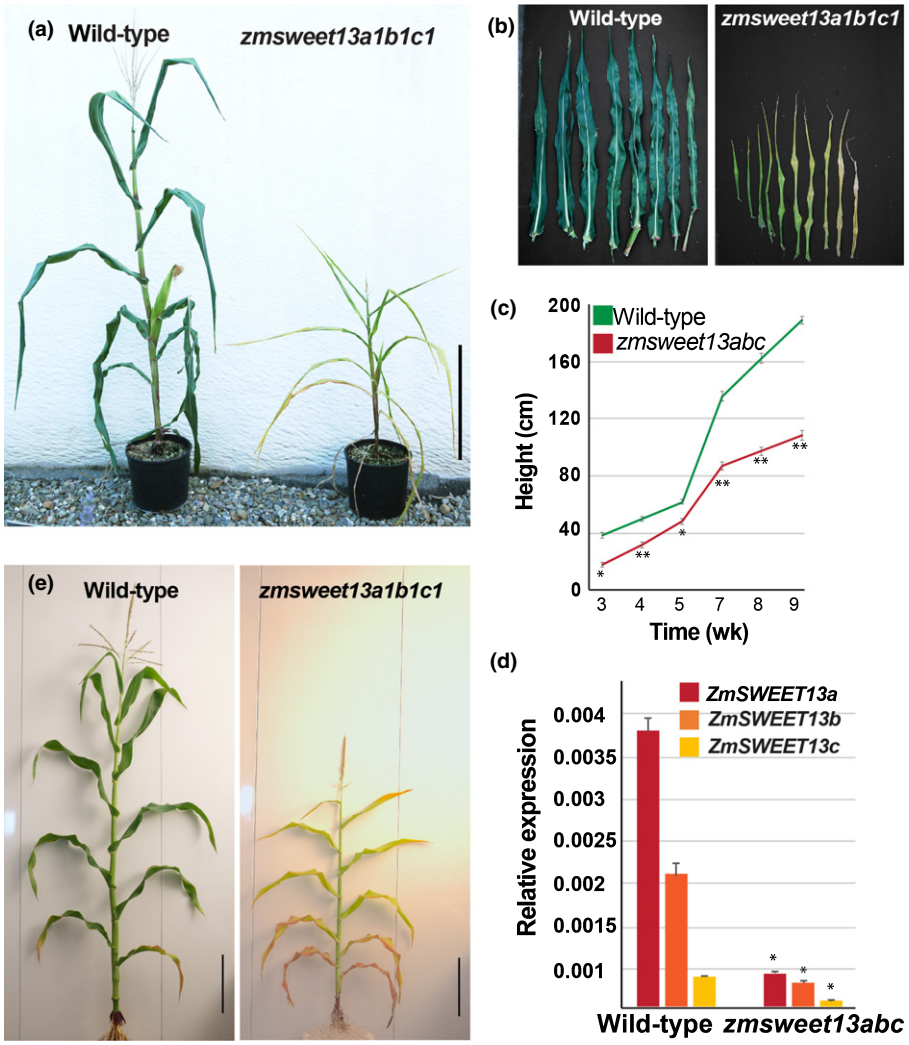

Fig. 4 Characterization *of ZmSWEET13abc* triple *Zea mays* L. mutants. (a) Mature wild-type and same-age *zmsweet13a1b1c1* triple mutant, showing reduced growth and leaf chlorosis. Bar, 50 cm. (b) Leaf phenotype of plants presented in Fig. 2(a), showing reduced length, width and chlorosis in leaves of the *zmsweet13a1b1c1* triple mutant. (c) Growth of wild-type and triple mutants in glasshouse conditions (mean ± SEM, $n = 17$ and 15, two-tailed *t*-test performed between wild-type and *zmsweet13abc*: *, $P < 0.005$; **, $P < 0.001$). (d) Relative mRNA levels (by qRT-PCR) of *ZmSWEET13* paralogs in maize flag leaves from wild-type and *zmsweet13abc*. Samples were harvested at 16:00 h (mean ± SEM, $n = 3$ technical replicates with expression normalized to 18S levels, repeated independently five times with comparable results, see Fig. S13(e, f)). Two-tailed *t*-test performed between wild-type and *zmsweet13abc* for each gene: four pools of four (16 plants) for each genotype: *, $P < .0001$. (e) Mature field-grown *zmsweet13a1b4c1* plants under field conditions (Carnegie field 2016). Mutants were stunted, showed severe chlorosis of all leaves, and anthocyanin accumulation in the oldest leaves.

Brachypodium and rice each have only one. The comparatively high number of *SWEET13s* had been attributed to specific roles in C_4 photosynthesis (Emms *et al.*, 2016), but the presence of three *SWEET13s* in *T. urartu* (Fig. 1a), the progenitor of the A-genome of bread wheat *T. aestivum*, both of which are C_3 plants, puts this interpretation into question. Evidence that maize SWEET13s cooperate in phloem loading is based on two key observations: the severe growth defect of *zmsweet13abc* mutants is similar to that of *zmsut1* mutants (Slewinski *et al.*, 2009), and a massive accumulation of free sugars and starch in leaves is also consistent with a defect in phloem translocation. These phenotypic effects are also similar to the RNAi-mediated SUT1 knockdown phenotypes in potato and tobacco (Riesmeier *et al.*, 1994; Bürkle *et al.*, 1998). The observed growth defect in maize is much more severe than that of the *atsweet11;12* mutant in Arabidopsis, and comparable to that of the *zmsut1* mutant (Slewinski *et al.*, 2009; Chen *et al.*, 2012). We thus propose that the three ZmSWEET13s and ZmSUT1 play dominant roles in phloem loading, probably in the same pathway.

Notably, the combined *zmsweet13abc* mutations were not lethal, because the plants still produced fertile viable offspring, implying compensatory or alternative mechanisms for phloem loading. While it is possible that other transporters might compensate, it is unlikely that other clade III SWEETs take over such roles, as judged by the lack of induction of other clade III SWEET genes in the mutants. Maize may thus either also have parallel symplasmic or other yet unknown loading mechanisms.

It is still not clear whether *SWEET13* triplication mainly serves to increase the amount of SWEET protein in the same cells (e.g. phloem parenchyma), or if each SWEET13 transporter mediates

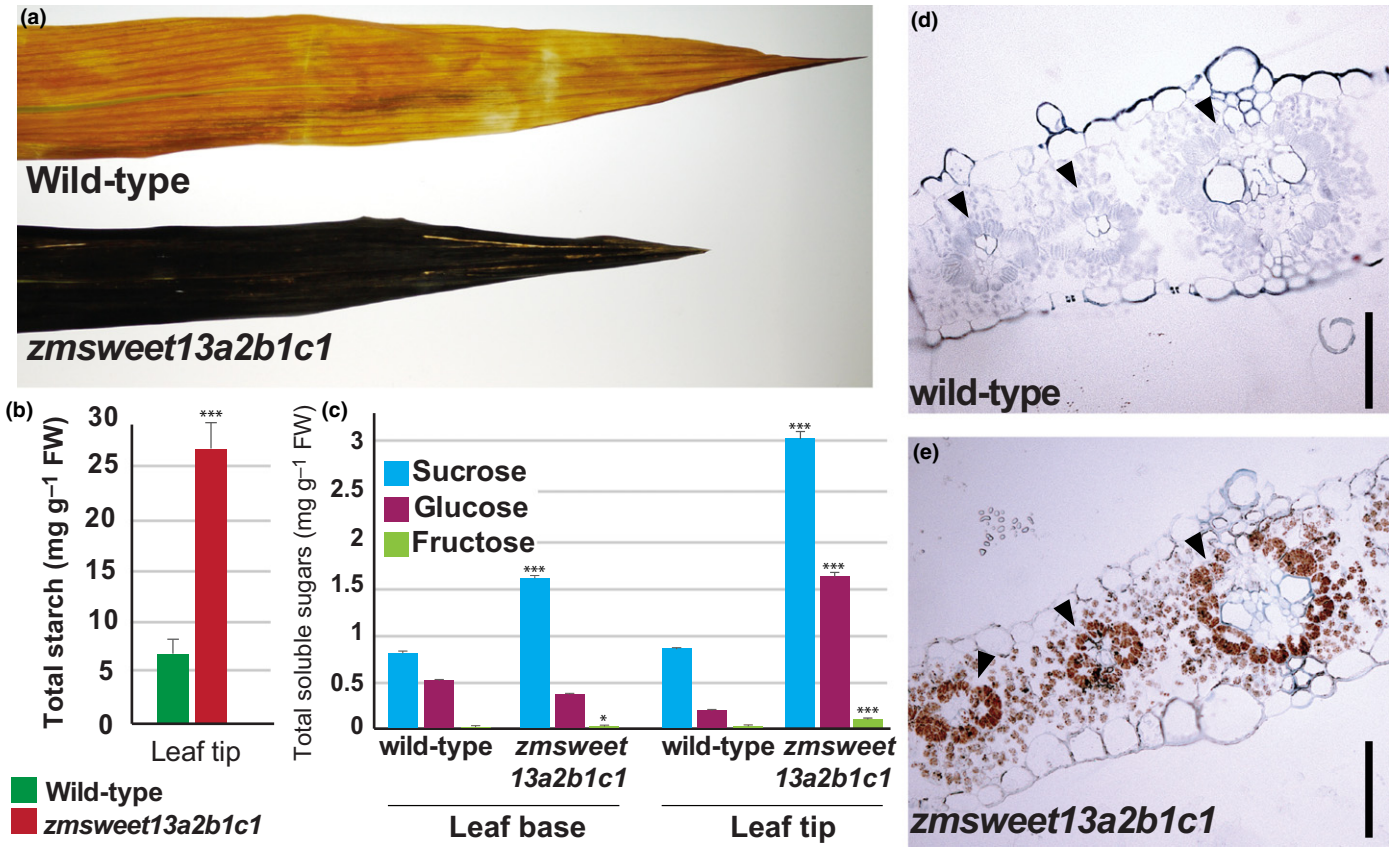

Fig. 5 Starch and soluble sugar accumulation in *zmsweet13abc Zea mays* L. triple mutants. (a) Flag leaves were collected at dawn (07:00 h), cleared with boiling ethanol and stained for 15 min with Lugol's solution. (b) Starch quantification from the same leaves as displayed in (a). The triple mutant contained ~5× more starch compared to wild-type in leaf tips. No significant differences were measured in the sheath or base (mean ± SEM, two-tailed *t*-test performed between wild-type and *zmsweet13abc*: *, $P < 0.05$; **, $P < 0.001$; ***, $P < 0.0001$; $n = 3$ technical replicates, repeated independently three times with comparable results, see Fig. S13a, b). (c) Quantification of soluble sugars in the flag leaf of *zmsweet13a2b1c1* mutants. The triple mutant contained higher sugar levels in both tip and base of the leaf. Samples were harvested at 07:00 h (mean ± SEM, two-tailed *t*-test performed between wild-type and *zmsweet13abc* for each sugar: *, $P < 0.05$; **, $P < 0.001$; ***, $P < 0.0001$; $n = 3$ technical replicates, repeated independently three times with comparable results, see Fig. S13b,c). (d, e) Starch accumulation in leaves from wild-type (d) and the triple mutant (e) harvested at the end of the night. Leaves were fixed, embedded and stained with Lugol's solution for starch. Starch grains accumulated in both mesophyll and bundle sheath cells in the *zmsweet13a2b1c1* mutant, while wild-type controls showed no detectable starch accumulation at this time point (arrowheads indicate vascular bundles). Bar, 75 mm.

efflux from a specific cell type and loading is achieved in a multi-tier manner. This question is of particular interest because *in situ* hybridization experiments identified SUT1 in companion cells, xylem and phloem parenchyma, as well as bundle sheath (Baker *et al.*, 2016). With the intent of localizing SWEET13 paralogs, we had generated translational reporter gene fusions that included the first three introns. However, neither GUS activity nor GFP fluorescence were detectable in any of the transformants carrying fusions for either of the three SWEET13s (data not shown). We therefore hypothesize that additional regulatory elements that were lacking from our chimeras must be required for proper expression.

Another interesting question is whether maize can serve as a model for phloem loading in rice, barley and wheat. Surprisingly, RNAi of the rice homolog of *ZmSUT1* did not lead to a detectable effect on the phenotype of the sporophyte (Ishimaru *et al.*, 2001). Thus, it remains a matter of debate whether rice uses predominantly apoplasmic and symplasmic or other mechanisms simultaneously (Eom *et al.*, 2012; Braun *et al.*, 2014). It will therefore be important to study the role of SWEET homologs in rice and other crops. It is noteworthy in this context that the clade III sucrose transporters OsSWEET11 and 15 are expressed preferentially in the caryopsis and act as key players in apoplasmic unloading processes in developing rice grains (Ma *et al.*, 2017; Yang *et al.*, 2018).

Data from the GWAS analysis indicate that genetic variation at the *ZmSWEET13s* loci in the maize diversity panels is significantly associated with several phenotypic traits, including ear- and developmental-related traits. Although the causality needs to be validated, the identified SNP markers might be useful for marker-assisted selection for further crop improvement. A better understanding of the role of SWEET sugar transporters in phloem loading in maize may guide future engineering efforts to improve yield potential.

Acknowledgements

We thank Joelle Sasse, Bi-Huei Hou, Aurélie Grimault, Franklin Talavera-Rauh, Xiao-Qing Xu, Grayson Badgley and Guido Grossmann for experimental support during various analyses. We thank Ari Kornfeld (Department of Global Ecology,

Carnegie Science) for help and advice with photosynthesis measurements. This work was made possible by research grants from Syngenta Crop Protection, LLC (WBF), the Office of Basic Energy Sciences of the US Department of Energy (DE-FG02-04ER15542; W.B.F.), the Bill and Melinda Gates Foundation, and the National Science Foundation (IOS-1258018; B.Y., W.B.F.). W.B.F.'s lab is supported by the Alexander von Humboldt Foundation.

Author contributions

M.B., S.N.C., B.Y., W.B.F. and D.S. conceived and designed experiments. M.B., M.H., T.H., S.N.C., B.Y. and D.S. performed experiments. M.B., T.H., B.Y., J.Y., W.B.F. and D.S. analysed the data. D.S. and W.B.F. wrote the manuscript, M.B. and B.Y. helped with revisions.

Competing financial interests

The authors (D.S. and W.B.F., on behalf of Carnegie Science) have filed a PCT patent application based in part on this work with the US Patent and Trademark Office.

References

Ainsworth EA, Bush DR. 2011. Carbohydrate export from the leaf: a highly regulated process and target to enhance photosynthesis and productivity. *Plant Physiology* **155**: 64.

Baker RF, Leach KA, Boyer NR, Swyers MJ, Benitez-Alfonso Y, Skopelitis T, Luo A, Sylvester A, Jackson D, Braun DM. 2016. Sucrose transporter ZmSut1 expression and localization uncover new insights into sucrose phloem loading. *Plant Physiology* **172**: 1876–1898.

Benjamini Y, Hochberg Y. 1995. Controlling the false discovery rate: a practical and powerful approach to multiple testing. *Journal of the Royal Statistical Society Series B (Methodological)* **57**: 289–300.

Botha CEJ. 2013. A tale of two neglected systems-structure and function of the thin- and thick-walled sieve tubes in monocotyledonous leaves. *Frontiers in Plant Science* **4**: 297.

Braun DM, Wang L, Ruan Y-L. 2014. Understanding and manipulating sucrose phloem loading, unloading, metabolism, and signalling to enhance crop yield and food security. *Journal of Experimental Botany* **65**: 1713–1735.

Bukowski R, Guo X, Lu Y, Zou C, He B, Rong Z, Wang B, Xu D, Yang B, Xie C *et al.* 2017. Construction of the third generation *Zea mays* haplotype map. *GigaScience*: gix134.

Bürkle L, Hibberd JM, Quick WP, Kühn C, Hirner B, Frommer WB. 1998. The H^+-sucrose cotransporter NtSUT1 is essential for sugar export from tobacco leaves. *Plant Physiology* **118**: 59–68.

Chang Y-M, Liu W-Y, Shih AC-C, Shen M-N, Lu C-H, Lu M-YJ, Yang H-W, Wang T-Y, Chen SC-C, Chen SM *et al.* 2012. Characterizing regulatory and functional differentiation between maize mesophyll and bundle sheath cells by transcriptomic analysis. *Plant Physiology* **160**: 165.

Char SN, Neelakandan AK, Nahampun H, Frame B, Main M, Spalding MH, Becraft PW, Meyers BC, Walbot V, Wang K *et al.* 2017. An *Agrobacterium*-delivered CRISPR/Cas9 system for high-frequency targeted mutagenesis in maize. *Plant Biotechnology Journal* **15**: 257–268.

Chardon F, Bedu M, Calenge F, Klemens PA, Spinner L, Clement G, Chietera G, Leran S, Ferrand M, Lacombe B *et al.* 2013. Leaf fructose content is controlled by the vacuolar transporter SWEET17 in Arabidopsis. *Current Biology* **23**: 697–702.

Chen L-Q, Cheung LS, Feng L, Tanner W, Frommer WB. 2015a. Transport of sugars. *Annual Review of Biochemistry* **84**: 865–894.

Chen LQ, Hou BH, Lalonde S, Takanaga H, Hartung ML, Qu XQ, Guo WJ, Kim JG, Underwood W, Chaudhuri B *et al.* 2010. Sugar transporters for intercellular exchange and nutrition of pathogens. *Nature* **468**: 527–532.

Chen H-Y, Huh J-H, Yu Y-C, Ho L-H, Chen L-Q, Tholl D, Frommer WB, Guo W-J. 2015b. The Arabidopsis vacuolar sugar transporter SWEET2 limits carbon sequestration from roots and restricts *Pythium* infection. *Plant Journal* **83**: 1046–1058.

Chen LQ, Qu XQ, Hou BH, Sosso D, Osorio S, Fernie AR, Frommer WB. 2012. Sucrose efflux mediated by SWEET proteins as a key step for phloem transport. *Science* **335**: 207–211.

Cohn M, Bart RS, Shybut M, Dahlbeck D, Gomez M, Morbitzer R, Hou B-H, Frommer WB, Lahaye T, Staskawicz BJ. 2014. *Xanthomonas axonopodis* virulence is promoted by a transcription activator-like effector-mediated induction of a SWEET sugar transporter in cassava. *Molecular Plant–Microbe Interactions: MPMI* **27**: 1186–1198.

Cox KL, Meng F, Wilkins KE, Li F, Wang P, Booher NJ, Carpenter SCD, Chen L-Q, Zheng H, Gao X *et al.* 2017. TAL effector driven induction of a SWEET gene confers susceptibility to bacterial blight of cotton. *Nature Communications* **8**: 15588.

Denton AK, Maß J, Külahoglu C, Lercher MJ, Bräutigam A, Weber APM. 2017. Freeze-quenched maize mesophyll and bundle sheath separation uncovers bias in previous tissue-specific RNA-Seq data. *Journal of Experimental Botany* **68**: 147–160.

Dobin A, Davis CA, Schlesinger F, Drenkow J, Zaleski C, Jha S, Batut P, Chaisson M, Gingeras TR. 2013. STAR: ultrafast universal RNA-seq aligner. *Bioinformatics* **29**: 15–21.

Dupree P, Pwee K-H, Gray JC. 1991. Expression of photosynthesis gene-promoter fusions in leaf epidermal cells of transgenic tobacco plants. *Plant Journal* **1**: 115–120.

Eggermont K, Goderis IJ, Broekaert WF. 1996. High-throughput RNA extraction from plant samples based on homogenisation by reciprocal shaking in the presence of a mixture of sand and glass beads. *Plant Molecular Biology* **14**: 273–279.

Emms DM, Covshoff S, Hibberd JM, Kelly S. 2016. Independent and parallel evolution of new genes by gene duplication in two origins of C_4 photosynthesis provides new insight into the mechanism of phloem loading in C_4 species. *Molecular Biology and Evolution* **33**: 1796–1806.

Eom J-S, Choi S-B, Ward JM, Jeon J-S. 2012. The mechanism of phloem loading in rice (*Oryza sativa*). *Molecules and Cells* **33**: 431–438.

Feng L, Frommer WB. 2015. Structure and function of SemiSWEET and SWEET sugar transporters. *Trends in Biochemical Sciences* **40**: 480–486.

Flint-Garcia SA, Thuillet A-C, Yu J, Pressoir G, Romero SM, Mitchell SE, Doebley J, Kresovich S, Goodman MM, Buckler ES. 2005. Maize association population: a high-resolution platform for quantitative trait locus dissection. *Plant Journal* **44**: 1054–1064.

Gottwald JR, Krysan PJ, Young JC, Evert RF, Sussman MR. 2000. Genetic evidence for the in planta role of phloem-specific plasma membrane sucrose transporters. *Proceedings of the National Academy of Sciences, USA* **97**: 13979–13984.

Guo W-J, Nagy R, Chen H-Y, Pfrunder S, Yu Y-C, Santelia D, Frommer WB, Martinoia E. 2014. SWEET17, a facilitative transporter, mediates fructose transport across the tonoplast of Arabidopsis roots and leaves. *Plant Physiology* **164**: 777–789.

Han L, Zhu Y, Liu M, Zhou Y, Lu G, Lan L, Wang X, Zhao Y, Zhang XC. 2017. Molecular mechanism of substrate recognition and transport by the AtSWEET13 sugar transporter. *Proceedings of the National Academy of Sciences, USA* **114**: 10089–10094.

Ishimaru K, Hirose T, Aoki N, Takahashi S, Ono K, Yamamoto S, Wu J, Saji S, Baba T, Ugaki M *et al.* 2001. Antisense expression of a rice sucrose transporter OsSUT1 in rice (*Oryza sativa* L.). *Plant & Cell Physiology* **42**: 1181–1185.

Joung J-G, Corbett AM, Fellman SM, Tieman DM, Klee HJ, Giovannoni JJ, Fei Z. 2009. Plant MetGenMAP: an integrative analysis system for plant systems biology. *Plant Physiology* **151**: 1758.

Kanno Y, Oikawa T, Chiba Y, Ishimaru Y, Shimizu T, Sano N, Koshiba T, Kamiya Y, Ueda M, Seo M. 2016. AtSWEET13 and AtSWEET14 regulate gibberellin-mediated physiological processes. *Nature Communications* **7**: 13245.

Klemens PAW, Patzke K, Deitmer J, Spinner L, Le Hir R, Bellini C, Bedu M, Chardon F, Krapp A, Neuhaus HE. 2013. Overexpression of the vacuolar sugar carrier AtSWEET16 modifies germination, growth, and stress tolerance in Arabidopsis. *Plant Physiology* **163**: 1338–1352.

Latorraca NR, Fastman NM, Venkatakrishnan AJ, Frommer WB, Dror RO, Feng L. 2017. Mechanism of substrate translocation in an alternating access transporter. *Cell* **169**: 96–107.

Li P, Ponnala L, Gandotra N, Wang L, Si Y, Tausta SL, Kebrom TH, Provart N, Patel R, Myers CR *et al.* 2010. The developmental dynamics of the maize leaf transcriptome. *Nature Genetics* **42**: 1060–1067.

Lin IW, Sosso D, Chen L-Q, Gase K, Kim S-G, Kessler D, Klinkenberg PM, Gorder MK, Hou B-H, Qu X-Q *et al.* 2014. Nectar secretion requires sucrose phosphate synthases and the sugar transporter SWEET9. *Nature* **508**: 546–549.

Love MI, Huber W, Anders S. 2014. Moderated estimation of fold change and dispersion for RNA-seq data with DESeq2. *Genome Biology* **15**: 550.

Ma L, Zhang D, Miao Q, Yang J, Xuan Y, Hu Y. 2017. Essential role of sugar transporter OsSWEET11 during the early stage of rice grain filling. *Plant & Cell Physiology* **58**: 863–873.

Purcell S, Neale B, Todd-Brown K, Thomas L, Ferreira MAR, Bender D, Maller J, Sklar P, de Bakker PIW, Daly MJ *et al.* 2007. PLINK: a tool set for whole-genome association and population-based linkage analyses. *American Journal of Human Genetics* **81**: 559–575.

Regmi KC, Zhang S, Gaxiola RA. 2016. Apoplasmic loading in the rice phloem supported by the presence of sucrose synthase and plasma membrane-localized proton pyrophosphatase. *Annals of Botany* **117**: 257–268.

Riesmeier JW, Willmitzer L, Frommer WB. 1994. Evidence for an essential role of the sucrose transporter in phloem loading and assimilate partitioning. *EMBO Journal* **13**: 1–7.

Scofield GN, Hirose T, Gaudron JA, Furbank RT, Upadhyaya NM, Ohsugi R. 2002. Antisense suppression of the rice transporter gene, OsSUT1, leads to impaired grain filling and germination but does not affect photosynthesis. *Functional Plant Biology* **29**: 815–826.

Slewinski TL, Meeley R, Braun DM. 2009. Sucrose transporter1 functions in phloem loading in maize leaves. *Journal of Experimental Botany* **60**: 881–892.

Sosso D, Luo D, Li Q-B, Sasse J, Yang J, Gendrot G, Suzuki M, Koch KE, McCarty DR, Chourey PS *et al.* 2015. Seed filling in domesticated maize and rice depends on SWEET-mediated hexose transport. *Nature Genetics* **47**: 1489–1493.

Srivastava AC, Dasgupta K, Ajieren E, Costilla G, McGarry RC, Ayre BG. 2009. Arabidopsis plants harbouring a mutation in AtSUC2, encoding the predominant sucrose/proton symporter necessary for efficient phloem transport, are able to complete their life cycle and produce viable seed. *Annals of Botany* **104**: 1121–1128.

Sun MX, Huang XY, Yang J, Guan YF, Yang ZN. 2013. Arabidopsis RPG1 is important for primexine deposition and functions redundantly with RPG2 for plant fertility at the late reproductive stage. *Plant Reproduction* **26**: 83–91.

Tausta SL, Li P, Si Y, Gandotra N, Liu P, Sun Q, Brutnell TP, Nelson T. 2014. Developmental dynamics of Kranz cell transcriptional specificity in maize leaf reveals early onset of C_4-related processes. *Journal of Experimental Botany* **65**: 3543–3555.

Turgeon R, Wolf S. 2009. Phloem transport: cellular pathways and molecular trafficking. *Annual Review of Plant Biology* **60**: 207–221.

Wang L, Czedik-Eysenberg A, Mertz RA, Si Y, Tohge T, Nunes-Nesi A, Arrivault S, Dedow LK, Bryant DW, Zhou W *et al.* 2014. Comparative analyses of C_4 and C_3 photosynthesis in developing leaves of maize and rice. *Nature Biotechnology* **32**: 1158.

Xuan YH, Hu YB, Chen LQ, Sosso D, Ducat DC, Hou BH, Frommer WB. 2013. Functional role of oligomerization for bacterial and plant SWEET sugar transporter family. *Proceedings of the National Academy of Sciences, USA* **110**: E3685–E3694.

Yang J, Luo D, Yang B, Frommer WB, Eom J-S. 2018. SWEET11 and 15 as key players in seed filling in rice. *New Phytologist* **218**: 604–615.

Zhou X, Stephens M. 2012. Genome-wide efficient mixed-model analysis for association studies. *Nature Genetics* **44**: 821–824.

Zhu XG, Long SP, Ort DR. 2010. Improving photosynthetic efficiency for greater yield. *Annual Review of Plant Biology* **61**: 235–261.

Supporting Information

Additional Supporting Information may be found online in the Supporting Information tab for this article:

Fig. S1 Expression pattern of SWEET genes in *Zea mays* L. across four leaf-specific RNA-seq datasets.

Fig. S2 Chromosomal localization and potential synteny of *ZmSWEET13s* in *Zea mays* L. and *Oryza sativa*.

Fig. S3 SWEET13 orthologs in different grasses.

Fig. S4 Expression of *ZmSWEET13a*, *b* and *c* in sink and source tissues of *Zea mays* L.

Fig. S5 Photosynthetic rates in *Zea mays* L. *zmsweet13abc* mutants.

Fig. S6 *ZmSWEET* mRNA levels in *Zea mays* L. *zmsweet13abc* mutants.

Fig. S7 Principal component analysis of differentially expressed genes in *zmsweet13* mutants and wild type

Fig. S8 Differentially expressed genes in *Zea mays* L. *zmsweet13abc* mutants involved in light-harvesting processes.

Fig. S9 Differentially expressed genes in *Zea mays* L. *zmsweet13abc* mutants involved in chlorophyll and tetrapyrrole biosynthesis.

Fig. S10 Differentially expressed genes in *Zea mays* L. *zmsweet13abc* mutants involved in sucrose and starch biosynthesis.

Fig. S11 GWAS results for *ZmSWEET13c* genes in *Zea mays* L.

Fig. S12 GWAS results for ZmSWEET13a and ZmSWEET13b genes in *Zea mays* L.

Fig. S13 Biological repeats of sugar quantification and qRT-PCR of *Zea mays* L. leaves.

Table S1 List of primers

Table S2 Read statistics of RNA-seq experiments

Table S3 Significantly affected pathways in *Zea mays* L. zm*sweet-13abc* mutants

Please note: Wiley Blackwell are not responsible for the content or functionality of any Supporting Information supplied by the authors. Any queries (other than missing material) should be directed to the *New Phytologist* Central Office.

SUPPORTING INFORMATION

Impaired phloem loading in zmsweet13a,b,c sucrose transporter triple *knock-out* mutants in *Zea mays*

Accepted: 28 December 2017

Margaret Bezrutczyk[1,2], Thomas Hartwig[1,2], Marc Horschman[2], Si Nian Char[3], Jinliang Yang[4], Bing Yang[3], Wolf B. Frommer[1,2,§] and Davide Sosso[2,5]

[1] Institute for Molecular Physiology, Heinrich Heine University Düsseldorf 40225, and Max Planck Institute for Plant Breeding Research, Cologne 50829, Germany.

[2] Department of Plant Biology, Carnegie Science, 260 Panama St., Stanford, CA 94305, USA

[3] Department of Genetics, Development, and Cell Biology, Iowa State University, Ames, IA 50011, USA

[4] Department of Agronomy and Horticulture, University of Nebraska-Lincoln, Lincoln, NE 68588, USA

[5] Inari Agriculture Inc., Cambridge, MA, 02139, USA

[§] For correspondence: frommew@hhu.de; +49 211 8114826

The following Supporting Information is available for this article:

Figure S1. Expression pattern of SWEET genes in *Zea mays* L. across four leaf-specific RNA-seq datasets.

Figure S2. Chromosomal localization and potential synteny of *ZmSWEET13s* in *Zea mays* L. and *Oryza sativa.*

Figure S3. SWEET13 orthologues in different grasses.

Figure S4. Expression of *ZmSWEET13a*, *b*, and *c* in sink and source tissues of *Zea mays* L.

Figure S5. Photosynthetic rates in *Zea mays* L. *zmsweet13abc* mutants.

Figure S6. *ZmSWEET* mRNA levels in *Zea mays* L. *zmsweet13abc* mutants.

Figure S7. Distribution of RNAseq samples and differentially expressed genes in *Zea mays* L.

Figure S8. Differentially expressed genes in *Zea mays* L. *zmsweet13abc* mutants involved in light harvesting processes.

Figure S9. Differentially expressed genes in *Zea mays* L. *zmsweet13abc* mutants involved in chlorophyll and tetrapyrrole biosynthesis.

Figure S10. Differentially expressed genes in *Zea mays* L. *zmsweet13abc* mutants involved in sucrose and starch biosynthesis.

Figure S11. GWAS results for *ZmSWEET13c* genes in *Zea mays* L.

Figure S12. GWAS results for ZmSWEET13a and ZmSWEET13b genes in *Zea mays* L.

Figure S13. Biological repeats of sugar quantification and qRT-PCR of *Zea mays* L. leaves.

Table S1. List of primers

Table S2. Read statistics of RNAseq experiments in *Zea mays* L.

Table S3. Significantly affected pathways in *Zea* mays L. *sweet13abc* mutants

		TPM Denton et al., 2016		TPM Tausta et al., 2014		TPM Chang et al., 2012		TPM Li et al., 2010	
		Mesophyll	Bundle Sheath	Mesophyll	Bundle Sheath	Mesophyll	Bundle Sheath	Mesophyll	Bundle Sheath
ZmSWEET1a	GRMZM2G039365	0.51	2.14	0.00	0	0.66	3.40	0.82	0.38
ZmSWEET1b	GRMZM2G153358	12.74	2.16	0.07	0.04	7.61	32.21	1.08	0.32
ZmSWEET2	GRMZM2G324903	1.44	2.46	0.34	0.21	7.12	5.58	2.47	0.92
ZmSWEET3a	GRMZM2G179679	0	0.01	0	0	0.11	0.47	0	0
ZmSWEET3b	GRMZM2G060974	0	0	0	0	0	0	0	0
ZmSWEET4a	GRMZM2G000812	0.10	0.60	0.03	0.03	0.19	0.17	0.15	0
ZmSWEET4b	GRMZM2G144581	0.22	3.09	0.31	0.85	2.21	32.33	1.16	3.07
ZmSWEET4c	GRMZM2G137954	0	0	0	0	0.01	0.05	0	0
ZmSWEET6a	GRMZM2G157675	0	0	0	0	0.02	0.25	0	0.12
ZmSWEET6b	GRMZM2G416965	0	0	0	0	0	0	0	0
ZmSWEET11a	GRMZM2G368827	0	0	0	0	0	0	0.08	0
ZmSWEET11b	GRMZM5G872141	0	0	0	0	0	0	0	0
ZmSWEET12a	GRMZM2G133322	0	0	0	0	0	0	0	0
ZmSWEET12b	GRMZM2G099609	0	0	0	0	0	0	0	0
ZmSWEET13a	GRMZM2G173669	110.60	582.15	29.11	83.33	92.68	1306.79	59.77	173.79
ZmSWEET13b	GRMZM2G021706	25.32	127.24	53.58	199.05	35.41	512.93	79.02	428.84
ZmSWEET13c	GRMZM2G179349	98.25	479.85	1.72	10.22	109.45	1435.78	8.55	62.31
ZmSWEET14a	GRMZM2G094955	0	0	0	0	0.03	0.26	0.09	0
ZmSWEET14b	GRMZM2G015976	0	0	0.11	0.08	1.98	2.41	0	0
ZmSWEET15a	GRMZM2G168365	0	0	0	0	0	0	0.29	0
ZmSWEET15b	GRMZM5G872392	0	0	0.07	0.02	0.07	0.08	0.77	0.08
ZmSWEET16	GRMZM2G107597	0.05	0.16	0	0	0.10	0.05	0.27	0
ZmSWEET17a	GRMZM2G106462	19.33	10.48	0.08	0.19	0	0	0.78	1.74
ZmSWEET17b	GRMZM2G111926	5.36	4.81	0.43	0.22	2.84	2.42	2.77	0.77

Figure S1. Expression pattern of SWEET genes in *Zea mays* L. across four leaf-specific RNA-seq datasets.

ZmSWEET13a,b,c mRNAs preferentially accumulate in the bundle sheath and veins, rather than mesophyll cells in all four independent databases (Li *et al.*, 2010; Chang *et al.*, 2012; Tausta *et al.*, 2014; Denton *et al.*, 2017).

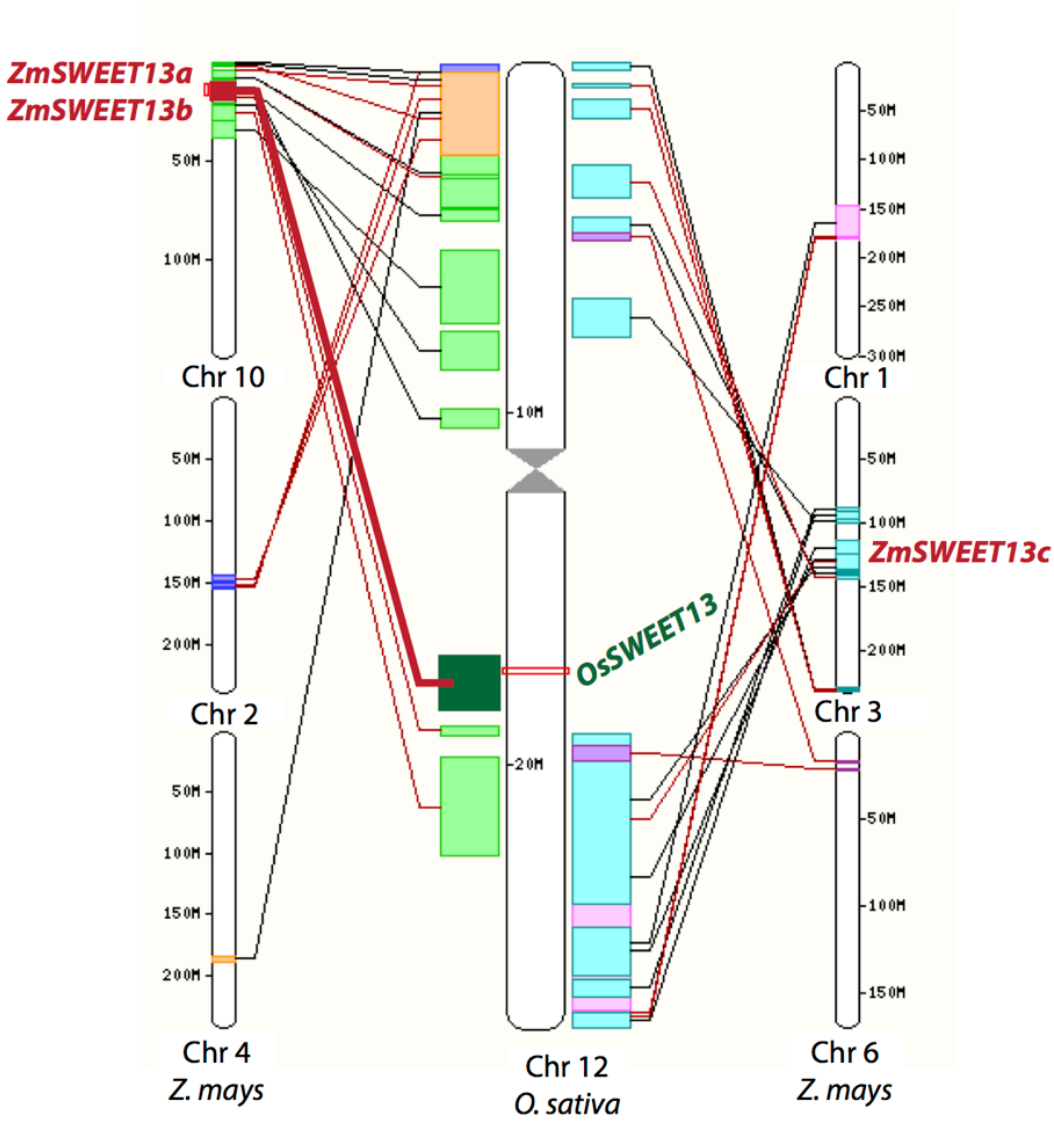

Figure S2. Chromosomal localization and potential synteny of *ZmSWEET13s* in *Zea mays* L. and *Oryza sativa*. *OsSWEET13* locus on rice chr12 (dark green box) is syntenic with the corresponding locus on maize chr10 (red box), where *ZmSWEET13*a and *ZmSWEET13b* are located. *ZmSWEET13c* is located on maize chr3, and might be the result of a more recent translocation event in maize or its ancestors.

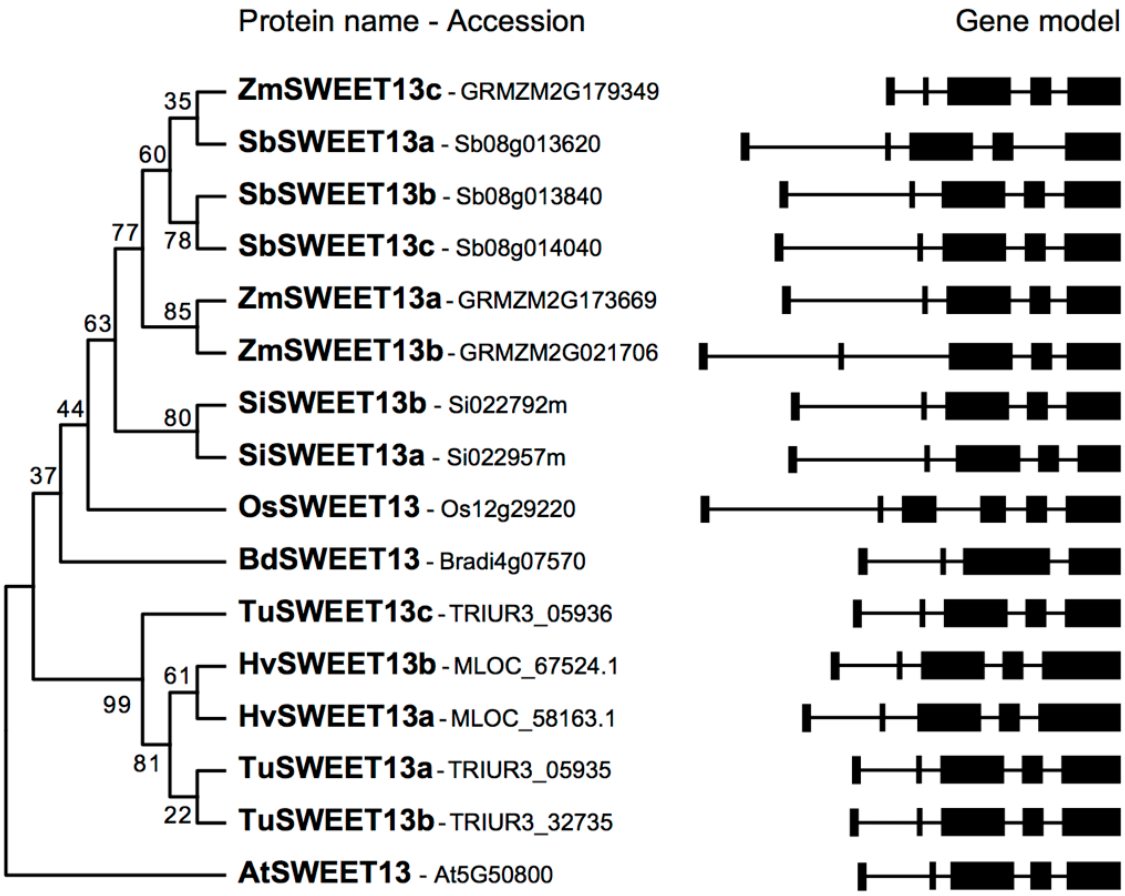

Figure S3. SWEET13 orthologs in different grasses.

Phylogenic tree of SWEET proteins collected from different grasses: *Zea mays* L. (Zm), *Oryza sativa* (Os, rice), *Sorghum bicolor* (Sb, sorghum), *Setaria italica* (Si; foxtail millet), *Brachypodium distachyon* (Bd, Brachypodium), *Hordeum vulgare* (Hv, barley) and *Triticum urartu* (Tu, wheat). *A. thaliana* was used as sole dicot out-group. Tree was inferred using Maximum likely-hood. Bootstrap values are out of 1000 replicates. Schematic of the *SWEET13* gene models across all species used in the tree (black boxes represent exons, lines represent introns).

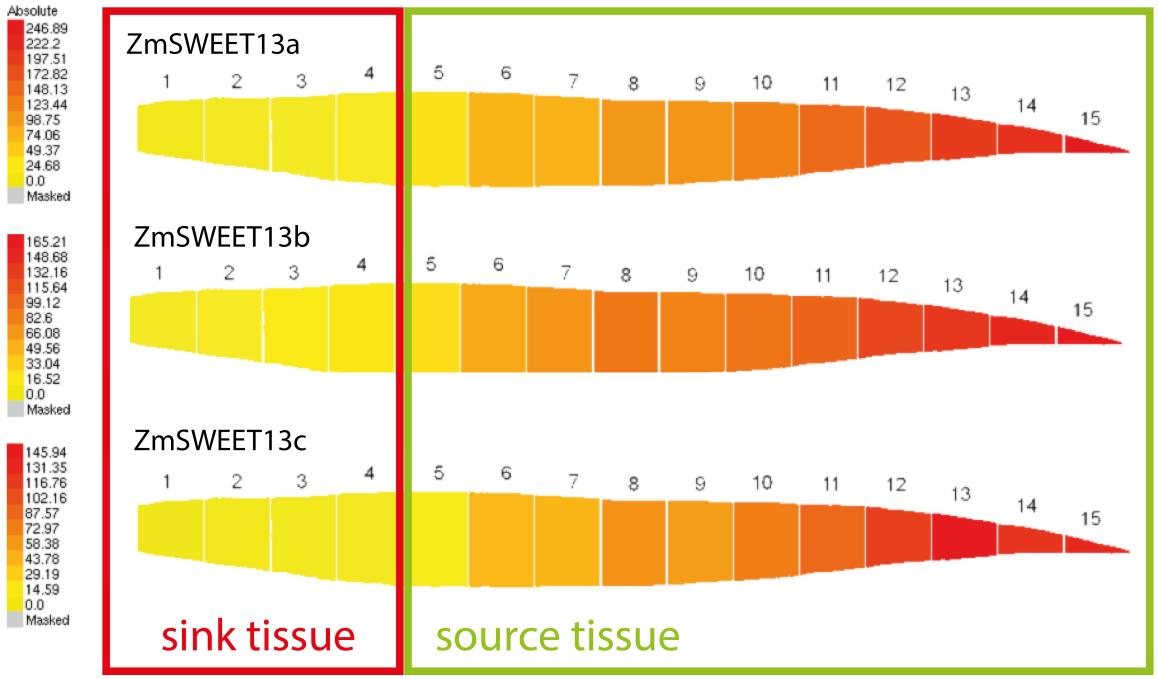

Figure S4. Expression of *ZmSWEET13a*, *b*, and *c* in sink and source tissues of *Zea mays L*.

Relative levels of ZmSWEET13 transcripts in 3rd leaf of juvenile maize plants. Wang et al 2014 determined source and sink segments using [^{14}C]-labelling and found that segments 1-4 represent sink tissue while 5-15 represent source tissue "Comparative analyses of C4 and C3 photosynthesis in developing leaves of maize and rice". SWEET13a, SWEET13b and SWEET13c all show dramatic increase in transcript levels at transition to from sink to source tissue. Scales show absolute transcript counts.

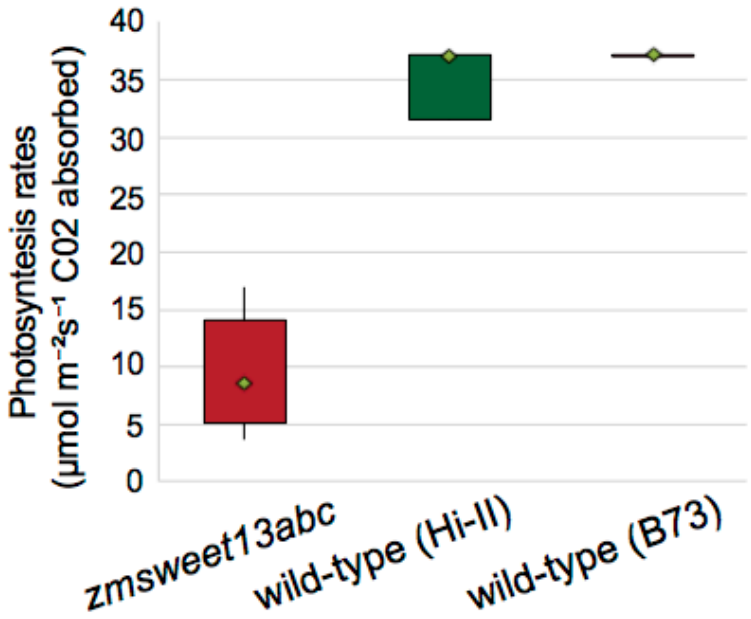

Figure S5. Photosynthetic rates in *Zea mays* L. *zmsweet13abc* mutants.

Licor LI-6800 measurements on greenhouse-grown plants were made in the 7th-10th leaf tip at mid-day (mean ± s.e.m., n=3 (*zmsweet13abc)*, 3 (wild-type Hi-II) and 1 (wild-type B73). Lower and upper limits of boxes represent first and third quartile, respectively. Whiskers represent highest and lowest values, diamonds the median.

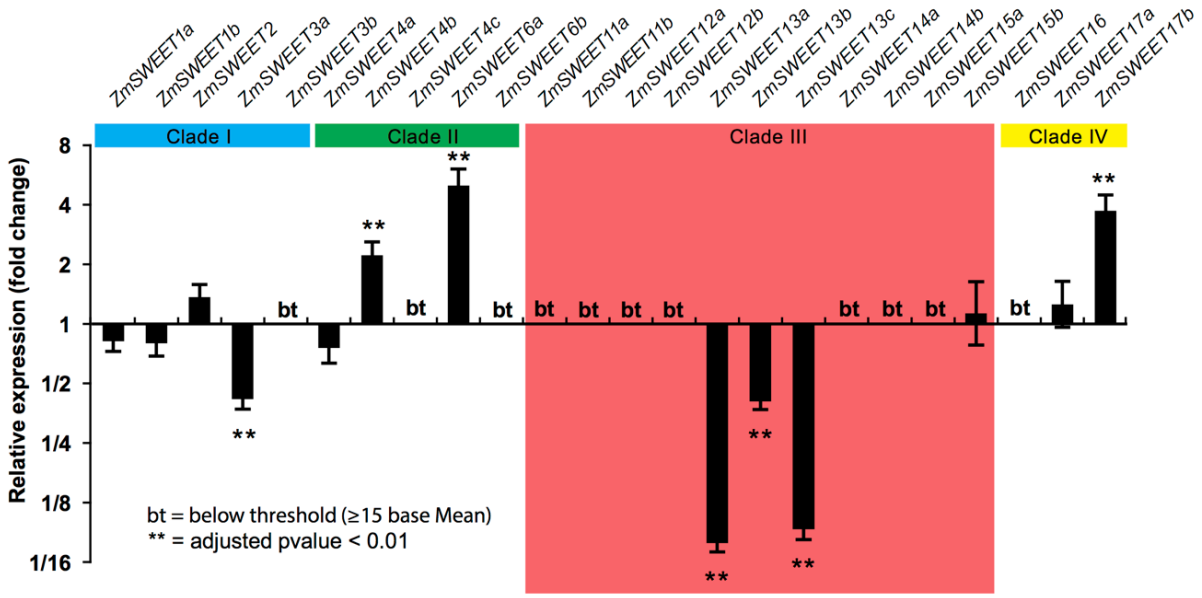

Figure S6. *ZmSWEET* mRNA levels in *Zea mays* L. *zmsweet13abc* mutants.

Relative expression of *SWEET* clade I-IV genes in *zmsweet13abc* mutant plants relative to wild type siblings. baseMean was calculated as the average of normalized count values taken over all samples. Error bars represent standard error of three biological replicates.

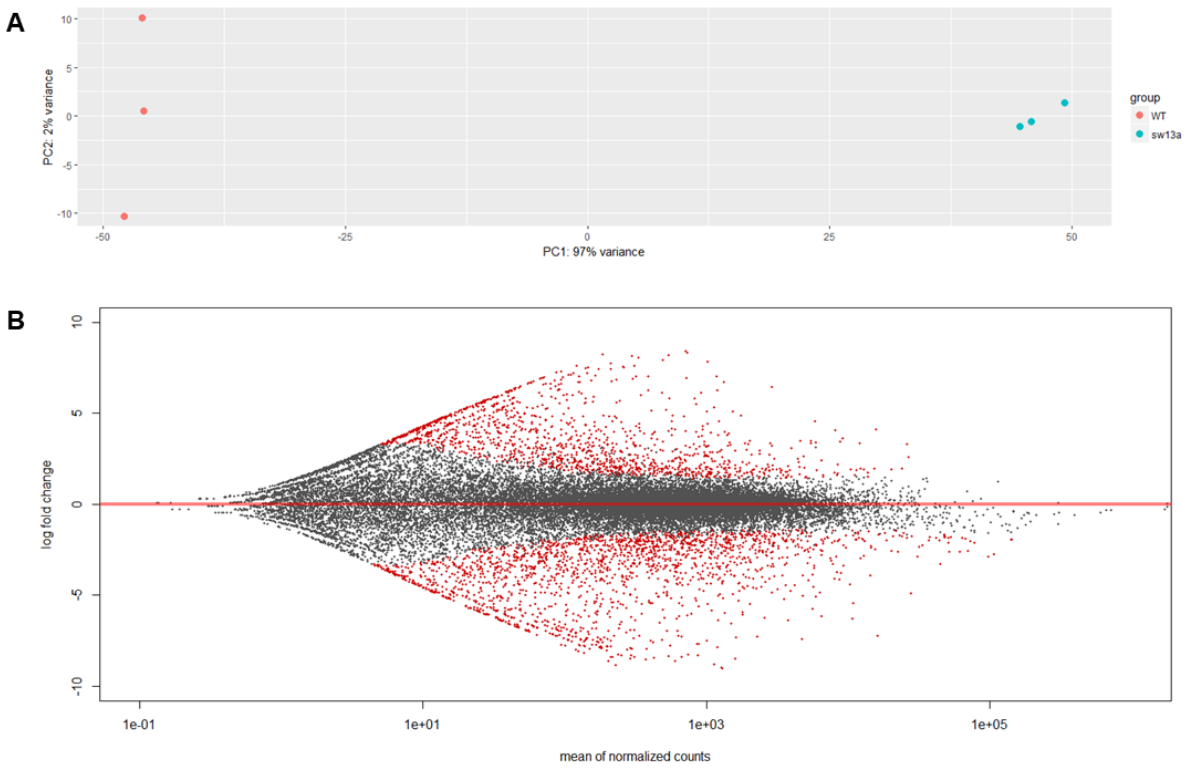

Figure S7. Distribution of RNAseq samples and differentially expressed genes in *Zea mays* L.

Principal component analysis of genes differentially expressed genes in *zmsweet13* mutants and wild type

(a) Principal component analysis plot using the rlog-transformed values for three replicates obtained with *zmsweet13abc* (turquoise) and wild type (red). **(b)** MA-plot of differentially expressed genes in zm*sweet13abc* versus wild type. Log2 fold change for mRNA levels in *sweet13abc* and wild type is plotted on the y-axis and the average of the counts normalized by size factor is shown on the x-axis. Each gene is represented with a dot. Differentially expressed genes with a *p*-value adjusted for multiple testing below 0.05 and above a twofold change in expression are shown in red.

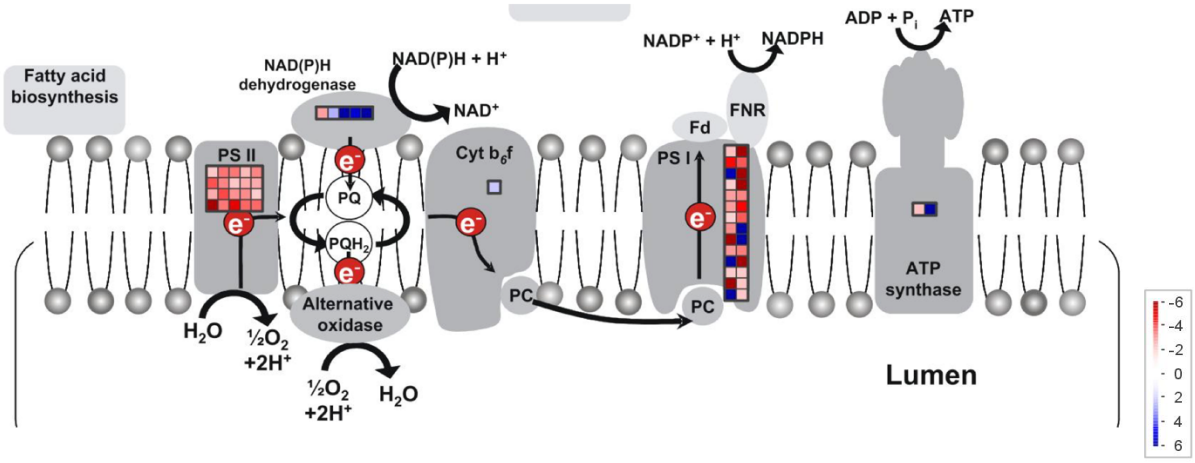

Figure S8. Differentially expressed genes in *Zea mays* L. *zmsweet13abc* mutants involved in light harvesting processes.

Differentially expressed genes (>2 fold, adj. p<0.05) in *zmsweet13abc* mutant plants relative to wild type siblings, were mapped (ZmB73_5b_2012) to MapMan (v. 3.6.0RC1) pathway of "ChloroPlast_CustomArray" in maize. Scale bar indicates fold change of downregulated (red) and upregulated (blue) genes in the mutant.

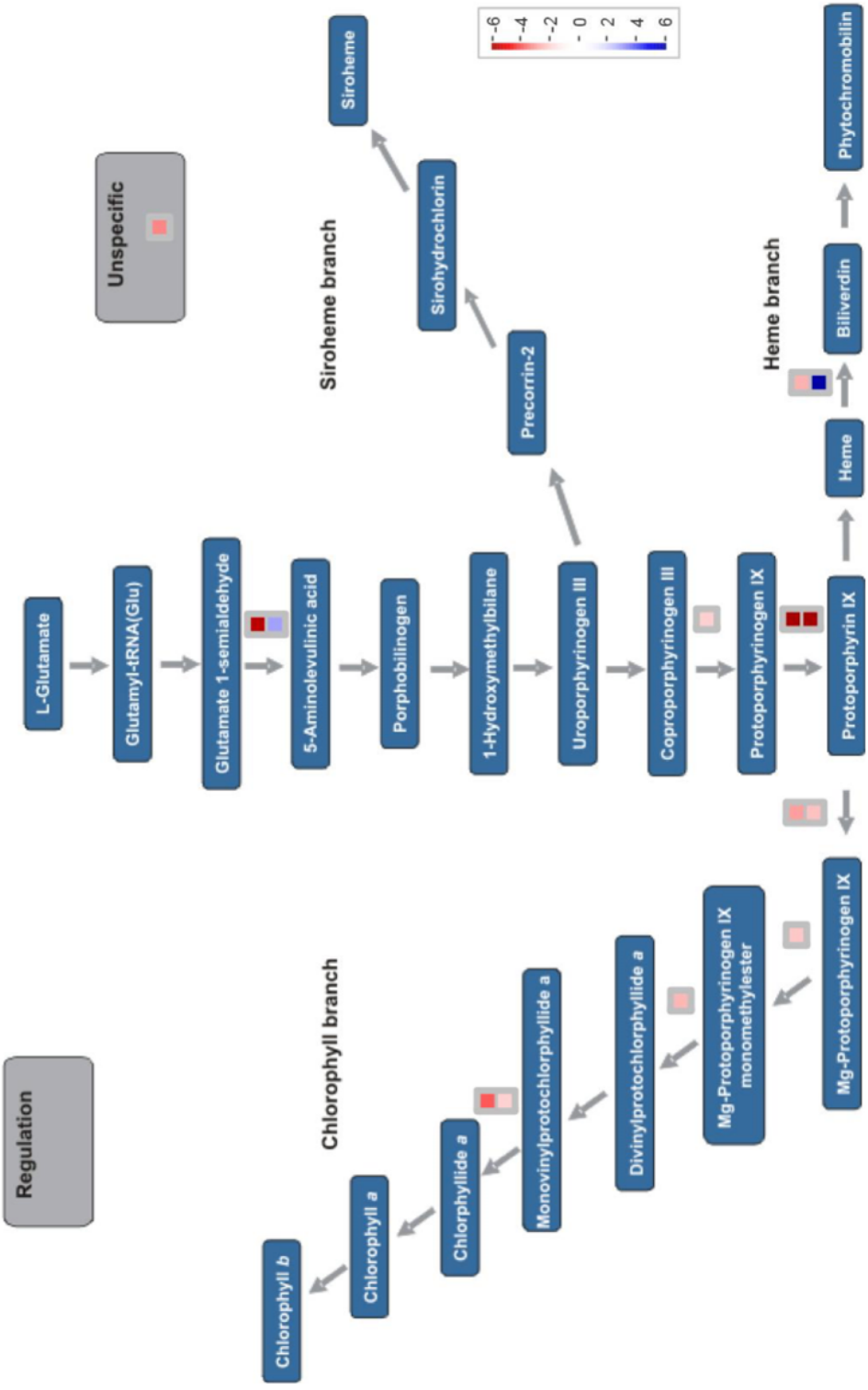

Figure S9. Differentially expressed genes in *Zea mays* L. *zmsweet13abc* mutants involved in chlorophyll and tetrapyrrole biosynthesis. Differentially expressed genes (>2 fold, adj. p<0.05) in *zmsweet13abc* mutant plants relative to wild type siblings, were mapped (ZmB73_5b_2012) to the MapMan (v. 3.6.0RC1) pathway of "tetrapyrrole biosynthesis" in maize. Scale bar indicates fold change of downregulated (red) and upregulated (blue) genes in the mutant.

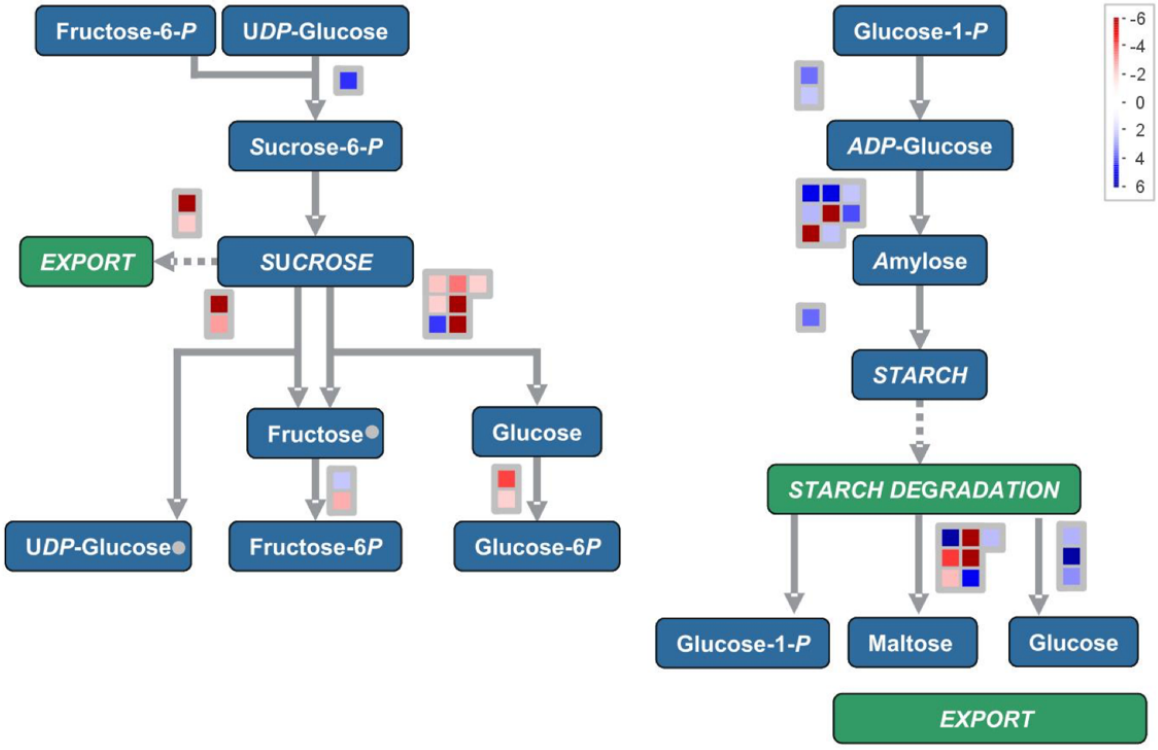

Figure S10. Differentially expressed genes in *Zea mays* L. *zmsweet13abc* mutants involved in sucrose and starch biosynthesis.

Differentially expressed genes (>2 fold, adj. p<0.05) in *zmsweet13* mutant plants versus wild type siblings, were mapped (ZmB73_5b_2012) to the MapMan (v. 3.6.0RC1) pathway of "sucrose and starch biosynthesis" in maize. Scale bar indicates fold change of downregulated (red) and upregulated (blue) genes in the mutant.

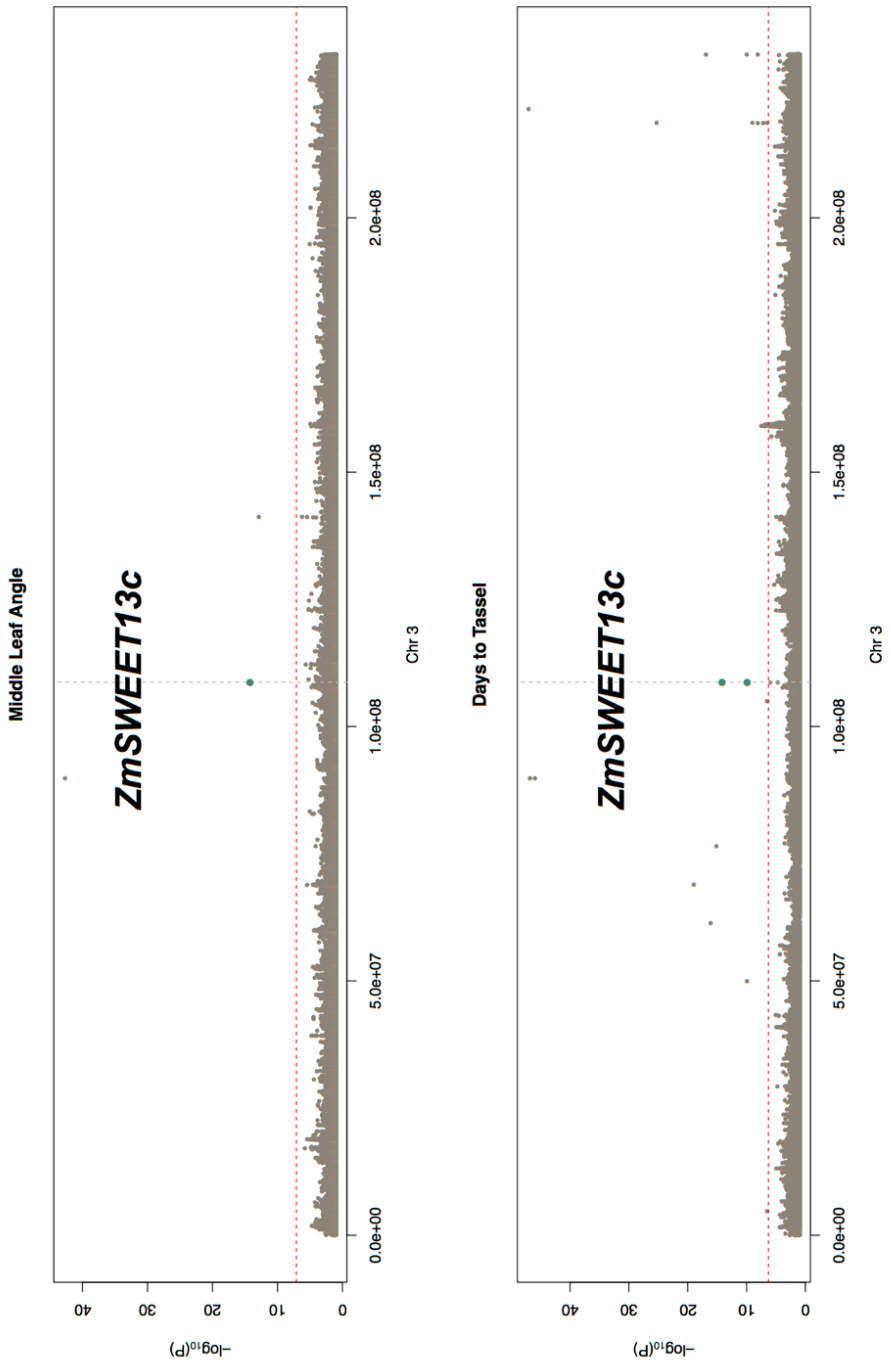

Figure S11. GWAS results for *ZmSWEET13c* genes in *Zea mays L.*

Horizontal red dashed lines denote the statistical threshold (FDR = 0.05). Significant SNPs in LD with *ZmSWEET13* genes are highlighted in green. Vertical dashed lines denote the physical location of *ZmSWEET13c* genes. Coordinates are based on AGPv3.

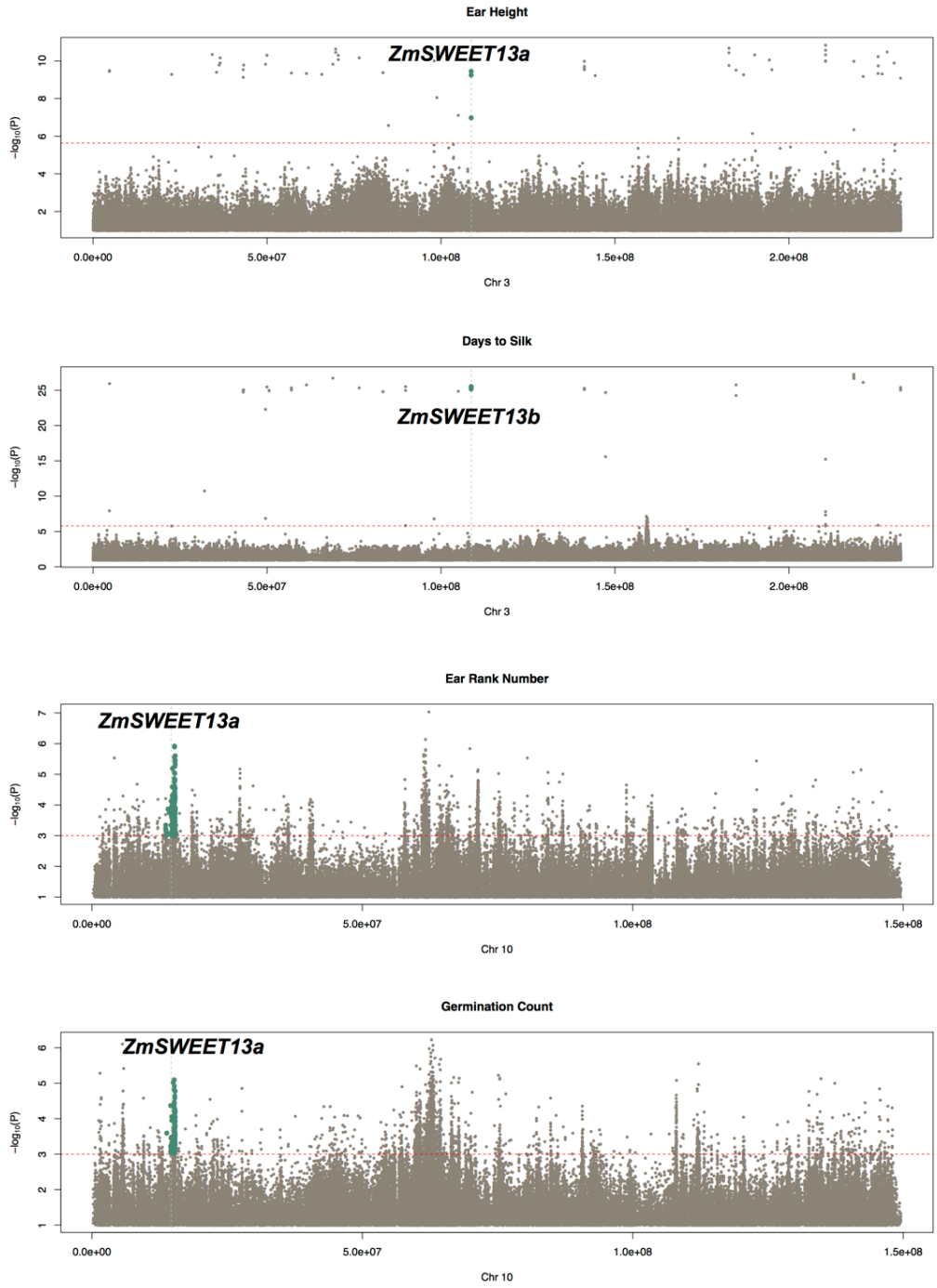

Figure S12. GWAS results for ZmSWEET13a and ZmSWEET13b genes in *Zea mays L*.

Horizontal red dashed lines denote the statistical threshold (FDR = 0.05). Significant SNPs in LD with *ZmSWEET13a* and *ZmSWEET13b* genes are highlighted in green. Vertical dashed lines denote the physical location of the *SWEET* genes. Coordinates are based on AGPv3.

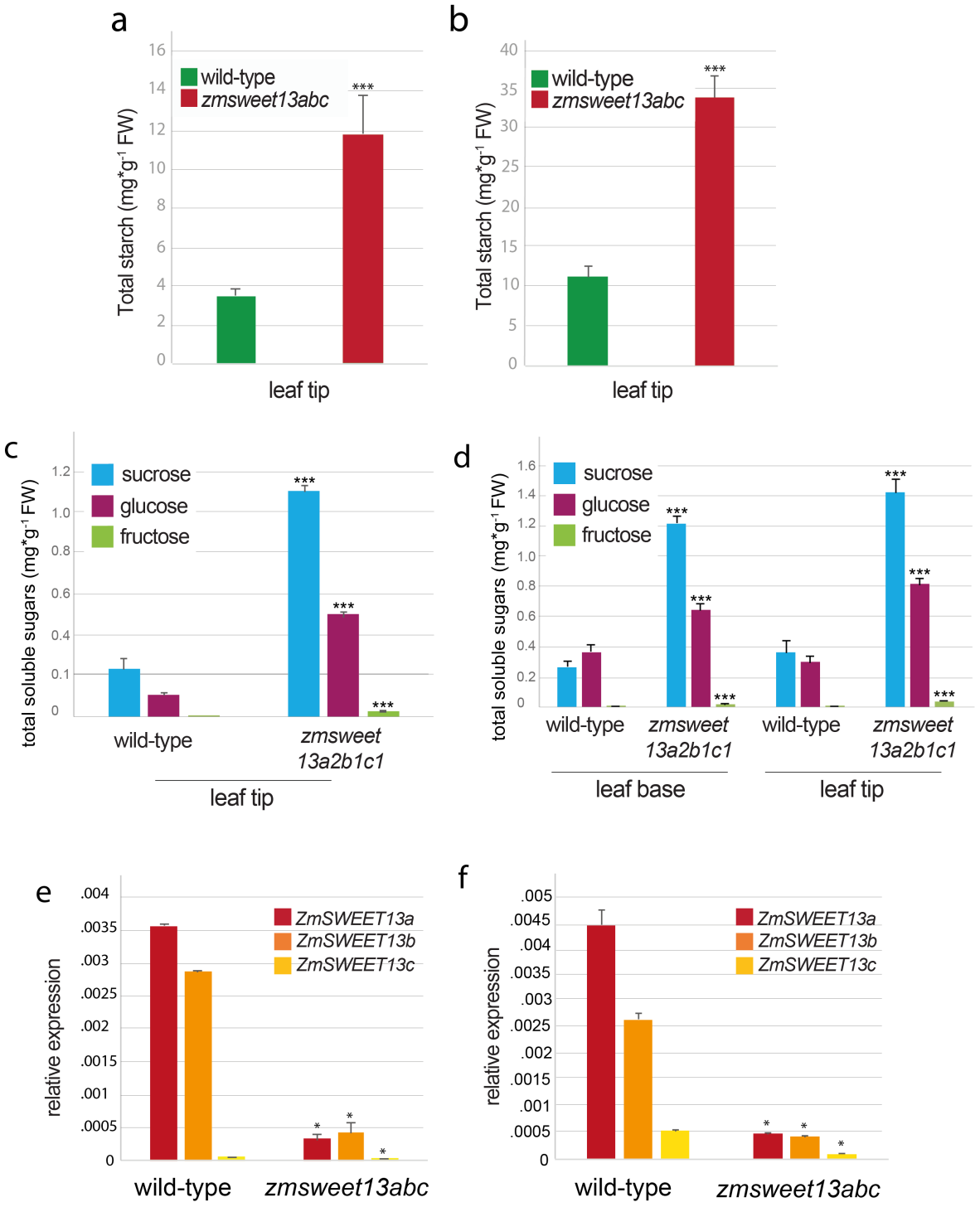

Figure S13. Biological repeats of sugar quantification and qRT-PCR of *Zea mays L.* leaves.

(A, B) Biological replicates of starch assay from Figure 5. Starch quantification of flag leaf tip from VT plant. The triple mutant shows 3x more starch than wild-type in the leaf tip (mean ± s.e.m., two-tailed t-test performed between wild type and *zmsweet13abc*; * $p<0.05$, ** $p<0.001$, *** $p<0.0001$)

(C,D) Biological replicates of soluble sugar assay from Figure 5. Soluble sugar measurements of wild-type and *zmsweet13a2b1c1* in maize flag leaf sections. The triple mutant shows higher sugar concentration in both the tip and the base of the leaf. Base of leaf measurements not available for second data set. Samples were harvested at 7:00 am (mean ± s.e.m., two-tailed t-test performed between wild type and *zmsweet13abc* for each sugar in the respective leaf sections; * $p<0.05$, ** $p<0.001$, *** $p<0.0001$)

(**E,F**) Biological replicates of qRT-PCR from Fig 2d. Relative expression (by qRT-PCR) of *ZmSWEET13* paralogs in maize flag leaf from wild-type and *zmsweet13abc*. Samples were harvested at 4:00 pm, expression normalized to 18S levels (mean ± s.e.m; two-tailed t-test performed between wild type and *zmsweet13abc* for each gene; *$p<0.0001$)

Table S1. List of primers

ZmSWT13a-F1	AATTATGTGGATATGTATGCATCG
ZmSWT13a-R1	GCGGTTGCAGCAGATTAGATG
ZmSWT13b-F1	AGTTTAGACGCGGTTGATGC
ZmSWT13b-R1	TGCATACAGACGACATCGCATG
ZmSWT13c-F1	TGAATCGAACCGTTAATTTGC
ZmSWT13c-R1	CATGATTTTGGCGGTGAACATC
ZmSweet13a_qF1	CAGACGAAGAGCGTGGAGTA
ZmSweet13a_qR1	GGTGAACCCCAGGA TGTTT
ZmSweet13b_qF1	CGCGCCACTAAGCATCAT
ZmSweet13b_qR1	GCTGAGGGTGAGCGAGAG
ZmSweet13c_qF1	CATTCACTTTCGGCCTCCTA
ZmSweet13c_qR1	ATGCGGTAGAACGTCGGTAT
Zm18s_qF	CCATCCCTCCGTAGTTAGCTT
Zm18s_qR	CCTGTCGGCCAAGGCTATATA
ZmLUG_qF	TCCAGTGCTACAGGGAAGGT
ZmLUG_qR	GTTAGTTCTTGAGCCCACGC
Cas9-1F	CATCGGTTGGAAGAATCGTT
Cas9-1R	CGCATTGATGGGATTCTCTT
Cas9-2F	CCAGCCTGGGTACGTATCAT
Cas9-2R	CGCTCCCTGCTATTTTTCTG
Cas9-3F	GTTGGGGATCACGATTATGG
Cas9-3R	AACTCGCTGATTTGCTCGAT

Table S2. Read statistics of RNAseq experiments in Zea mays L.

Sample	Raw reads	Filtered reads	Q30(%)	GC(%)	Unique mapped Reads	Unique mapping (%)
WT	36540317	35491274	92.29	60.67	34278170	93.81
WT	41386395	40111444	92.5	60.84	38878854	93.94
WT	40656975	39297057	93.91	59.41	38204086	93.97
sweet13abc	39679237	38473613	92.72	58.76	36556068	92.13
sweet13abc	45928549	44581202	91.85	58.83	42642931	92.85
sweet13abc	43235166	42017368	92.83	58.22	40254316	93.11

Table S3. Significantly affected pathways in *Zea* mays L. zm*sweet13abc* mutants

For pathway enrichment analysis the Plant MetGenMAP (Joung *et al.*, 2009) database with a significance cut-off of ≤ 0.05 was used and included all differentially expressed genes (fold change ≥ 2, adjusted p-value ≤ 0.05) between WT and sweet13abc plants.

up-reg. pathways in *sw13abc*	p value	down-reg. pathways in *sw13abc*	p value
suberin biosynthesis	4.0E-07	jasmonic acid biosynthesis	2.52E-03
phenylpropanoid biosynthesis (init. reactions)	1.8E-05	trehalose biosynthesis	7.66E-03
salicylate biosynthesis	3.0E-05	homogalacturonan degradation	1.20E-02
cellulose biosynthesis	1.5E-04	methanol oxidation to formaldehyde	1.60E-02
glycogen biosynthesis (from ADP-Glucose)	4.1E-04	cellulose biosynthesis	1.61E-02
methylthiopropionate biosynthesis	8.5E-04	divinyl ether biosynthesis (13-LOX)	1.70E-02
starch biosynthesis	9.5E-04	13-LOX and 13-HPL pathway	1.70E-02
homogalacturonan biosynthesis	1.1E-03	glycerol degradation	2.26E-02
methionine salvage pathway	2.6E-03	very long chain fatty acid biosynthesis	2.57E-02
free phenylpropanoid acid biosynthesis	3.6E-03	UDP-D-galacturonate biosynthesis (from UDP-D-glucuronate)	3.44E-02
methylquercetin biosynthesis	3.6E-03	abscisic acid glucose ester biosynthesis	3.84E-02
melibiose degradation	6.2E-03	superpathway of asparagine biosynthesis	3.84E-02
simple coumarins biosynthesis	1.1E-02	asparagine biosynthesis	3.84E-02
S-adenosyl-L-methionine cycle	1.8E-02	glutathione-mediated detoxification	3.84E-02
phenylpropanoid biosynthesis	3.5E-02	sucrose degradation I	4.00E-02
glyoxylate cycle	4.2E-02		
TCA cycle variation III (eukaryotic)	4.6E-02		

References

Chang Y-M, Liu W-Y, Shih AC-C, Shen M-N, Lu C-H, Lu M-YJ, Yang H-W, Wang T-Y, Chen SC-C, Chen SM, *et al.* 2012. Characterizing Regulatory and Functional Differentiation between Maize Mesophyll and Bundle Sheath Cells by Transcriptomic Analysis. *Plant Physiology* **160**: 165.

Denton AK, Maß J, Külahoglu C, Lercher MJ, Bräutigam A, Weber APM. **2017**. Freeze-quenched maize mesophyll and bundle sheath separation uncovers bias in previous tissue-specific RNA-Seq data. *Journal of Experimental Botany* **68**: 147–160.

Joung J-G, Corbett AM, Fellman SM, Tieman DM, Klee HJ, Giovannoni JJ, Fei Z. **2009**. Plant MetGenMAP: An Integrative Analysis System for Plant Systems Biology. *Plant Physiology* **151**: 1758.

Li P, Ponnala L, Gandotra N, Wang L, Si Y, Tausta SL, Kebrom TH, Provart N, Patel R, Myers CR, *et al.* 2010. The developmental dynamics of the maize leaf transcriptome. *Nat Genet* **42**: 1060–7.

Tausta SL, Li P, Si Y, Gandotra N, Liu P, Sun Q, Brutnell TP, Nelson T. **2014**. Developmental dynamics of Kranz cell transcriptional specificity in maize leaf reveals early onset of C4-related processes. *Journal of Experimental Botany* **65**: 3543–3555.